



# Distinct CIC-6 and CIC-7 Cl<sup>-</sup> sensitivities provide insight into CIC-7's role in lysosomal Cl<sup>-</sup> homeostasis

Maria Antonietta Coppola<sup>1,2</sup>, Paola Gavazzo<sup>1</sup>, Ilaria Zanardi<sup>1</sup>, Abraham Tettey-Matey<sup>1</sup>, Antonella Liantonio<sup>2</sup>, Peking Fong<sup>3</sup>  and Michael Pusch<sup>1</sup> 

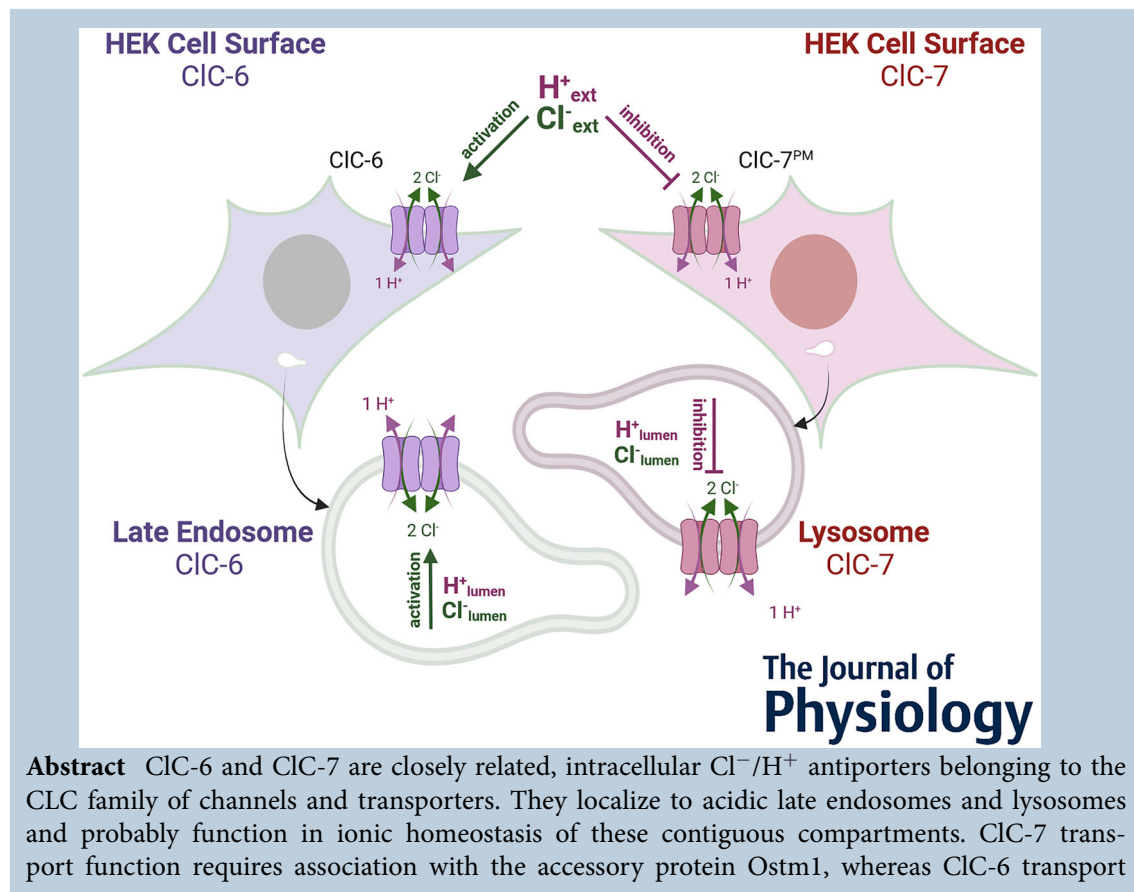
<sup>1</sup>Institute of Biophysics, CNR, Genoa, Italy

<sup>2</sup>Department of Pharmacy–Drug Sciences, University of Bari 'Aldo Moro', Bari, Italy

<sup>3</sup>Department of Anatomy and Physiology, Kansas State University College of Veterinary Medicine, Manhattan, Kansas, USA

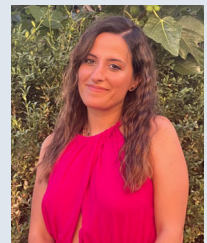
Handling Editors: David Wyllie & Péter Hegyi

The peer review history is available in the Supporting Information section of this article (<https://doi.org/10.1113/JP285431#support-information-section>).



**Abstract** CIC-6 and CIC-7 are closely related, intracellular Cl<sup>-</sup>/H<sup>+</sup> antiporters belonging to the CLC family of channels and transporters. They localize to acidic late endosomes and lysosomes and probably function in ionic homeostasis of these contiguous compartments. CIC-7 transport function requires association with the accessory protein Ostm1, whereas CIC-6 transport

**Maria Antonietta Coppola** achieved her masters degree in 'Chemistry and Pharmaceutical Technologies' from the University of Parma – Department of Food and Drug. During the second year of her PhD in Pharmacology – Drug Sciences at University of Bari 'Aldo Moro' she joined the lab of Dr Michael Pusch at the Italian National Research Council in Genoa for an internship period. Currently, she is starting as Researcher Fellow job position in the lab of Dr Michael Pusch. Her research fields of interest are focused on ion channels, particularly the family of CLC proteins.



does not. To elucidate their roles in endo-lysosomes, we measured  $\text{Cl}^-$  and pH-dependences of over-expressed wild-type CIC-6 and CIC-7, as well as disease-associated mutants, using high-resolution recording protocols. Lowering extracellular  $\text{Cl}^-$  (corresponding to luminal  $\text{Cl}^-$  in endo-lysosomes) reduced CIC-6 currents, whereas it increased transport activity of CIC-7/Ostm1. Low extracellular  $\text{Cl}^-$  activated CIC-7/Ostm1 under acidic extracellular conditions, as well as under conditions of low intracellular chloride. Activation is conserved in CIC-7<sup>Y713C</sup>, a variant displaying disrupted  $\text{PI}(3,5)\text{P}_2$  inhibition. Detailed biophysical analysis of disease-associated CIC-6 and CIC-7 gain-of-function (GoF) variants, CIC-6<sup>Y553C</sup> and CIC-7<sup>Y713C</sup>, and the CIC-7<sup>Y577C</sup> and CIC-6<sup>Y781C</sup> correlates, identified additional functional nuances distinguishing CIC-6 and CIC-7. CIC-7<sup>Y577C</sup> recapitulated GoF produced by CIC-6<sup>Y553C</sup>. CIC-6<sup>Y781C</sup> displayed transport activation qualitatively similar to CIC-7<sup>Y713C</sup>, although current density did not differ from that of wild-type CIC-6. Finally, rCIC-7<sup>R760Q</sup>, homologous to hCIC-7<sup>R762Q</sup>, an osteopetrosis variant with fast gating kinetics, appeared indifferent to extracellular  $\text{Cl}^-$ , identifying altered  $\text{Cl}^-$  sensitivity as a plausible mechanism underlying disease. Collectively, the present studies underscore the distinct roles of CIC-6 and CIC-7 within the context of their respective localization to late endosomes and lysosomes. In particular, we suggest the atypical inhibition of CIC-7 by luminal  $\text{Cl}^-$  serves to limit excessive intraluminal  $\text{Cl}^-$  accumulation.

(Received 2 August 2023; accepted after revision 16 October 2023; first published online 8 November 2023)

**Corresponding authors** P. Fong: Department of Anatomy and Physiology, Kansas State University College of Veterinary Medicine, Manhattan, KS, USA. Email: pfong@vet.k-state.edu; M. Pusch: Institute of Biophysics, CNR, Genoa, Italy. Email: michael.pusch@ibf.cnr.it

**Abstract figure legend** Plasma membrane-targeted CIC-6 and CIC-7 (top) produce whole cell currents characterized by opposite dependence on extracellular proton and chloride concentration. High extracellular chloride and proton concentrations (i.e. low pH) activate CIC-6 whereas they inhibit CIC-7. CIC-6 localizes to late endosomes whereas CIC-7 resides in lysosomes, and hence the physiological relevance of the extracellular conditions tested in the present studies apply to effects within the respective luminal compartments (bottom). The opposing regulation of these endolysosomal transporters by their substrates suggests non-overlapping physiological roles. Furthermore, these findings suggest that inhibition of CIC-7 by high luminal chloride may function to mitigate potentially disastrous osmotic effects of lysosomal chloride overload. Created with BioRender.com.

### Key points

- CIC-6 and CIC-7 are late endosomal and lysosomal  $2 \text{Cl}^- / 1 \text{H}^+$  exchangers, respectively. When targeted to the plasma membrane, both activate slowly at positive voltages.
- CIC-6 activity is decreased in low extracellular (i.e. luminal) chloride, whereas CIC-7 is activated by low luminal chloride, even at acidic pH.
- The functional gain-of-function phenotypes of the CIC-6 and CIC-7 disease mutations CIC-6<sup>Y553C</sup> and CIC-7<sup>Y713C</sup> are maintained when introduced in their respective homologues, CIC-7<sup>Y577C</sup> and CIC-6<sup>Y781C</sup>, with all mutations retaining chloride dependence of the respective wild type (WT).
- An osteopetrosis mutation of CIC-7 displaying fast gating kinetics (R762Q) was less sensitive to extracellular chloride compared to WT.
- The opposing substrate dependences of CIC-6 and CIC-7  $\text{Cl}^- / \text{H}^+$  exchangers point to non-overlapping physiological functions, leading us to propose that inhibition of CIC-7 by luminal chloride and protons serves to prevent osmotic stress imposed by hyper-accumulation of chloride.

### Introduction

The CLC family of anion transport proteins comprises both chloride channels and  $\text{Cl}^- / \text{H}^+$  antiporters residing

at plasma and intracellular membranes. Of the intracellular  $\text{Cl}^- / \text{H}^+$  antiporters, CIC-6 and CIC-7 share close homology and form a distinct branch, localizing to the adjoining, progressively more acidic, late endosomes and

lysosomes (Kasper et al., 2005; Kornak et al., 2001; Poët et al., 2006). Functionality of ClC-7 – but not ClC-6 – requires association with Ostm1, an accessory protein (Lange et al., 2006).

The acidic intra-compartmental pH of endosomes and lysosomes is critical for the chemical processes within these organelles, and Cl<sup>-</sup> fluxes probably function as important determinants for proper acidification (Jentsch, 2007; Mellman et al., 1986; Scheel et al., 2005). In a simple working model, luminal Cl<sup>-</sup> influx shunts the positive luminal potential resulting from active H<sup>+</sup> accumulation, thereby allowing efficient acidification. Indeed, flux studies performed in isolated lysosomes established a critical role for ClC-7-mediated, coupled Cl<sup>-</sup>/H<sup>+</sup> transport in promoting maximal acidification (Graves et al., 2008). In this respect it is interesting to note that acidic extracellular pH (pH<sub>ext</sub>), corresponding to luminal pH, actually diminishes transport currents of ClC-7/Ostm1 targeted to the plasma membrane by mutation of a lysosomal sorting motif (Leisle et al., 2011), similar to its effects on ClC-3, -4, and -5 transport currents (Jentsch & Pusch, 2018).

The structural homology and adjacent intracellular localization of ClC-6 and ClC-7/Ostm1 in late endosomes and lysosomes, respectively, suggested that they function similarly to sustain acidification or otherwise regulate endolysosomal ionic homeostasis. Until recently, measurements of ClC-6 were limited, hindering detailed interrogation of this prediction. The discovery that ClC-6 transport currents operate at extremely depolarized membrane potentials enabled the surprising discovery that wild-type ClC-6 is activated – rather than inhibited – by acidic pH<sub>ext</sub> (Zifarelli et al., 2022). Thus, ClC-6's pH dependence contrasts not only with ClC-7's, but also with that of ClC-3, -4, and -5, which form a distinct branch of intracellular CLCs (Friedrich et al., 1999; Picollo & Pusch, 2005; Picollo et al., 2010). These observations therefore suggest additional functional nuances distinguishing ClC-6 and ClC-7.

Interestingly, a neurodegenerative disease-associated, gain-of-function (GoF) variant, ClC-6<sup>Y553C</sup> (Polovitskaya et al., 2020), that strongly 'shifts' the voltage dependence of transport activation to less positive voltages (Zifarelli et al., 2022) preserves activation by low pH<sub>ext</sub>. However, the activating effect of pH<sub>ext</sub> is blunted for the mutation (Zifarelli et al., 2022). Tyrosine 553 localizes close the extracellular dimer interface, so it plausibly is positioned to function in pH<sub>ext</sub> sensing. Another interesting finding was that overexpression of ClC-6<sup>Y553C</sup> induced dramatic vacuolation of cells (Polovitskaya et al., 2020). In ClC-7, Y553 corresponds to Y577. Whether mutation of the tyrosine residue in ClC-7 similarly activates transport activity and alters pH dependence remains unknown.

In contrast, a disease-associated ClC-7 variant, ClC-7<sup>Y715C</sup>, localizes intracellularly to a region far

from that affected in ClC-6<sup>Y553C</sup> (Nicoli et al., 2019). GoF conferred by ClC-7<sup>Y715C</sup> was proposed to result from disruption of tonic inhibition by PI(3,5)P<sub>2</sub> (Leray et al., 2022). Whether ClC-7 inhibition by acidic pH<sub>ext</sub> is conserved in this variant thus far remains untested. Moreover, whether the corresponding residue in ClC-6, Y781, plays a similar role is unexplored.

Nonetheless, because they function as Cl<sup>-</sup>/H<sup>+</sup> exchangers, ClC-6 and ClC-7/Ostm1 probably are influenced not only by pH, but also by Cl<sup>-</sup> concentration ([Cl<sup>-</sup>]). Indeed, recent studies on ClC-7/Ostm1 point to its role in supporting lysosomal Cl<sup>-</sup> uptake, ensuring levels necessary for key degradative processes (Wu et al., 2023; Zhang et al., 2023). The opposing effects elicited by pH<sub>ext</sub> on transport currents carried by wild-type ClC-6 and ClC-7 (Pusch & Zifarelli, 2021; Zifarelli et al., 2022) led us to hypothesize that extracellular Cl<sup>-</sup> concentrations (corresponding to intraluminal Cl<sup>-</sup>) also exert differing effects on these transporters. Thus, to elucidate the role of ClC-6 and ClC-7 in maintaining endo-lysosomal ionic homeostasis, in the present studies we used high-resolution recording protocols to measure Cl<sup>-</sup> and pH-dependences of over-expressed wild-type and disease-associated mutants. For these studies, we use tagged constructs of the wild-type human ClC-6, as well as rat ClC-7, previously used in our laboratories to function indistinguishably from untagged human ClC-6 and human ClC-7.

Importantly, we found that reduction of extracellular Cl<sup>-</sup> reduced ClC-6 current, whereas it surprisingly increased transport activity of ClC-7/Ostm1, finally providing important insights into ClC-6's and ClC-7's distinct roles within the context of their respective localization to late endosomal and lysosomal compartments.

## Methods

### Wild-type expression constructs

GFP-tagged wild-type human ClC-6/pEGFP was the gift of Tobias Stauber and Thomas Jentsch (MSH Medical School Hamburg University of Applied Sciences and Medical University, Hamburg, Germany, and Max-Delbrück Centrum für Molekulare Medizin, Berlin, Germany). We previously demonstrated that currents mediated by untagged and tagged wild-type constructs do not differ (Zifarelli et al., 2022), and for convenience all ClC-6 variants tested in the present studies were based on the tagged construct. For experiments on ClC-7/Ostm1 function, we used a construct comprising mouse Ostm1, separated from plasma membrane-trafficking rat ClC-7 (rClC-7<sup>PM</sup>; (Stauber & Jentsch, 2010) by a self-cleaving peptide sequence. This was fused at the carboxyl terminus of ClC-7 to a E<sup>2</sup>GFP/DsRed fluorescence sensor and

placed in pFrog, an expression vector derived from pcDNA3 (Günther et al., 1998; Zanardi et al., 2013). For simplicity, we refer to this construct as CIC-7 throughout the present study, with variants referenced to the numbering of the rat CIC-7 sequence. Rat CIC-7 and human CIC-7 currents were found indistinguishable when over-expressed and measured in both amphibian and mammalian systems (Leisle et al., 2011).

### CIC-6 and CIC-7 variant constructs

All variants were generated by incorporating the desired mutations by PCR and subcloning the resultant fragments into the respective recipient plasmids. Variant plasmid constructs were produced either in-house or by outsourcing to GenScript (Piscataway, NJ, USA).

**CIC-6 constructs.** We further tested a human CIC-6 GoF variant, CIC-6<sup>Y553C</sup> (Polovitskaya et al., 2020; Zifarelli et al., 2022) (Fig. 1A). In addition, we tested CLC-6<sup>Y781C</sup> (Fig. 1A), corresponding to human CIC-7<sup>Y715C</sup>, a well-studied human lysosomal storage disease-associated CIC-7 GoF variant (hCIC-7<sup>Y715C</sup>) (Leray et al., 2022; Nicoli et al., 2019).

**CIC-7 constructs.** In our CIC-7 construct, Y577 corresponds to Y553 of hCIC-6 (Fig. 1A). We introduced cysteine at this position to produce a point mutant corresponding to human disease-associated CIC-6<sup>Y553C</sup>, CIC-7<sup>Y577C</sup>. In addition, for these studies we generated CIC-7<sup>Y713C</sup>, the rat equivalent of human disease-associated CIC-7<sup>Y715C</sup>. The third CIC-7 variant studied, CIC-7<sup>R760Q</sup>, corresponds to hCIC-7<sup>R762Q</sup> (Fig. 1A), a variant showing accelerated gating and associated with dominant osteopetrosis (Leisle et al., 2011).

### Mammalian cell culture and over-expression

HEK293 cells were cultured in media composed of Dulbecco's modified Eagle's medium with 1% glutamine, 1% penicillin/streptomycin, and 10% Fetal Bovine Serum (all from Euroclone), at 37°C, 5% CO<sub>2</sub>. HEK293 cells lacking TMEM206, which encodes the endogenous acid-sensitive, outwardly rectifying anion channels (ASOR) (Ullrich et al., 2019), were the gift of Thomas J. Jentsch (Leibniz-Forschungsinstitut für Molekulare Pharmakologie, and Max-Delbrück Centrum für Molekulare Medizin, Berlin, Germany). Expression plasmids were delivered to cells by transfection using a commercially available kit (Effectene; Qiagen).

### Electrophysiological measurements

Whole-cell current recordings were performed on HEK293 cells over-expressing wild-type and mutant constructs using established tight-seal recording procedures. Recording pipettes were pulled from borosilicate capillaries (Hilgenberg, Malsfeld, Germany), and in most studies filled with a standard intracellular

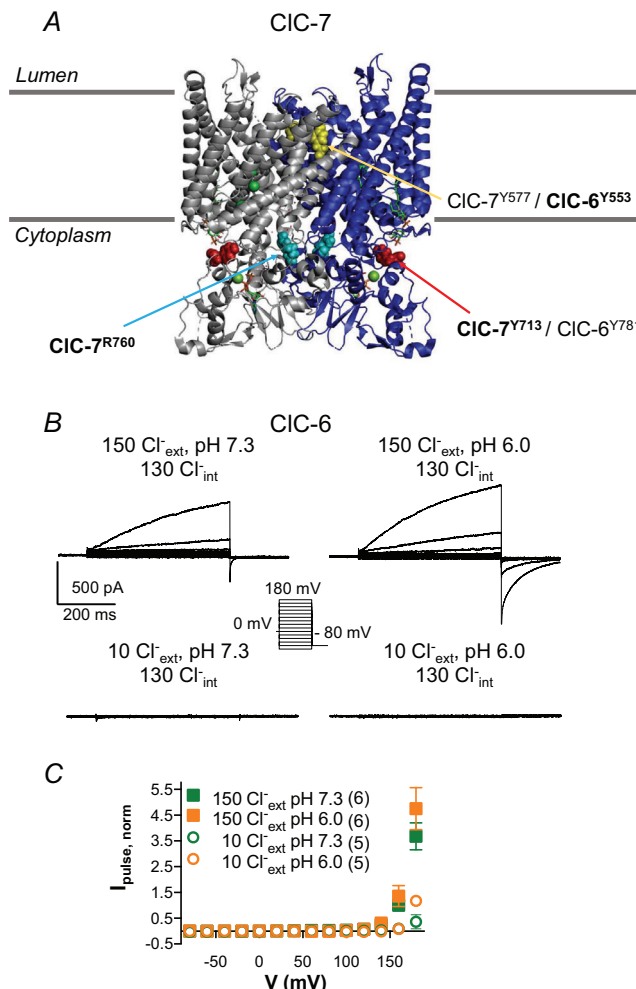


**Figure 1. Studied mutations mapped on CIC-7 structure, and effect of extracellular chloride and pH on CIC-6**

A, cartoon rendering depicts mutations studied in the context of the CIC-7 cryo-EM structure (PDB: 7JM7, from (Schrecker et al., 2020). Positions of disease-associated mutants bear boldface labelling and appear in coloured space-fill (yellow, CIC-6<sup>Y553C</sup>; red, CIC-7<sup>Y713C</sup>; aqua, CIC-7<sup>R760Q</sup>). Labelled also are the corresponding residues in either CIC-6 or CIC-7 evaluated in the present study. Green spheres indicate chloride ions within the permeation pathways. B and C illustrate typical currents indicative of CIC-6 inhibition by low extracellular Cl<sup>-</sup>. B, typical transport currents elicited by Protocol 2 (see inset), measured in the same cell perfused with: 150 mM Cl<sup>-</sup>, pH 7.3 (top left); 150 mM Cl<sup>-</sup>, pH 6.0 (top right); 10 mM Cl<sup>-</sup>, pH 7.3 (lower left); 10 mM Cl<sup>-</sup>, pH 6.0 (lower right). C shows a plot of normalized *I*-*V* relationship measured at the end of the test pulse; data are means ± SD. Number of cells for each condition is indicated in the figure key.



solution containing (in mM) 130 NaCl; 10 HEPES, 2 MgSO<sub>4</sub>, and 2 EGTA, pH 7.3. In standard extracellular solution (in mM: 150 NaCl, 10 HEPES, 4 calcium gluconate, 10 HEPES, 2 MgCl<sub>2</sub>, and 1 EGTA, pH 7.3), pipette resistances ranged between 1.5 and 3 MΩ. For recordings in acidic (pH 6 or pH 5) extracellular conditions, HEPES was replaced with MES. For low Cl<sup>-</sup> conditions, equimolar sodium glutamate substituted for NaCl. Extracellular solutions were exchanged by continuous perfusion via 0.5 mm diameter plastic tubing positioned close to the cell, with a 3 M KCl/1% agar bridge serving as ground.

Data were recorded by an Axopatch 200 amplifier (Molecular Devices), sampled at 100 kHz after filtering at 10 kHz by the amplifier-built-in 8-pole Bessel. Data were acquired using GePulse employing a National Instruments interface (NI PCI-6036), and analysis was performed with Ana, programs freely available from <http://users.ge.ibf.cnr.it/pusch>. SigmaPlot (Systat Software), and Prism (GraphPad) were used to perform additional analysis as needed.

Transient and transport currents were measured using voltage protocols described previously (Zifarelli et al., 2022), and appear as figure insets. Briefly, to acquire transient currents, 5 ms pulses were applied from a holding potential,  $V_{\text{hold}}$ , of 0 mV; these pulses progressed from 200 to 0 mV in 20 mV decrements (Protocol 1). A P/N subtraction procedure corrected for capacitive and leak currents within raw measurements. This entailed application of a scaled-down measurement protocol (0.2×), followed by suitable scaling and subtraction of the resultant currents from the raw currents.

Transport currents were measured using Protocol 2. From the 0 mV holding potential ( $V_{\text{hold}}$ ), we delivered 500 ms activating 'test' pulses to positive voltages ranging between 140 and 180 mV to -80 mV. For WT ClC-6 and ClC-6<sup>Y781C</sup>, the initial activating pulse was 180 mV (see inset in Fig. 1A), whereas it was 160 mV for ClC-6<sup>Y553C</sup> and ClC-7<sup>R780Q</sup>, and 140 mV for WT ClC-7, ClC-7<sup>Y577C</sup> and ClC-7<sup>Y713C</sup>. Activating pulses progressively hyperpolarized in decrements of 20 mV before applying a constant -80 mV 'tail' pulse. The initial peak inward currents in response to the -80 mV tail pulses were determined using a single exponential fit of the currents measured at -80 mV, followed by back-extrapolation to the pulse onset.

To discriminate the contributions of altered driving force vs. altered transporter activation, we applied Protocol 3. Currents were recorded while repetitively applying bipolar pulses from a holding potential of 0 mV (200 ms at 120 mV, followed by 100 ms at -80 mV; expanded waveforms shown as figure inset) and rapidly perfusing the bath with the specified test solutions of interest. In our system, solution exchange was achieved in less than 1 s.

## Data analysis

Quasi-steady state current-voltage relationships ( $I_{\text{ss}}-V$ ) plot normalized current values measured at the end of the test pulse as a function of test pulse potentials. Plotting initial peak inward tail currents at -80 mV against the respective test pulse potential yields the corresponding  $I_{\text{tail}}-V$ . Where indicated, normalized  $I$  values were applied in the analyses.

Resultant  $I_{\text{tail}}-V$  relationships were fitted by applying eqn (1), describing a Boltzmann function of the following form:

$$I(V) = \frac{I_{\text{max}}}{1 + e^{\frac{zF(V_{1/2}-V)}{RT}}}, \quad (1)$$

where  $z$  indicates the apparent gating valence,  $V_{1/2}$  represents the voltage at half-maximal activation; the Faraday constant, the gas constant, and the absolute temperature are denoted by  $F$ ,  $R$  and  $T$ , respectively. Note that the maximal current,  $I_{\text{max}}$ , was obtained by extrapolation, i.e. via the fitting procedure, and does not refer to the maximal measured current. For some conditions, the obtained  $V_{1/2}$  values are more positive than the maximally applied voltages. In these cases, in order to nevertheless obtain rather robust estimates of  $V_{1/2}$  and  $I_{\text{max}}$ , the gating valency,  $z$ , was fixed to value of 1, close to the value found in conditions of satisfactory saturation of the  $I_{\text{tail}}-V$  relationships for practically all constructs and conditions. Nevertheless, in cases of non-saturating  $I_{\text{tail}}-V$  relationships, the obtained values for  $V_{1/2}$  have to be considered as qualitative estimates.

Dependence of ClC-7 currents on extracellular Cl<sup>-</sup> was fitted assuming a simple inhibition of currents according to the expression (eqn 2a):

$$I(c) = \frac{I(0)}{1 + \frac{c}{K_D}}, \quad (2a)$$

with  $c$  being the Cl<sup>-</sup> concentration and  $K_D$  the apparent dissociation constant. Normalizing values to currents measured in 150 mM yields eqn (2b):

$$I_{\text{norm}}(c) = \frac{1 + \frac{150\text{mM}}{K_D}}{1 + \frac{c}{K_D}}. \quad (2b)$$

## Data representation and statistics

Data are reported as mean values ± the standard deviation (SD);  $n$  refers to the number of individual cells. Whenever possible, individual data points are included in data summaries. Tests of significance apply unpaired Student's  $t$  tests assuming equal variance. Unless < 0.001, exact  $P$  values are stated.

## Results

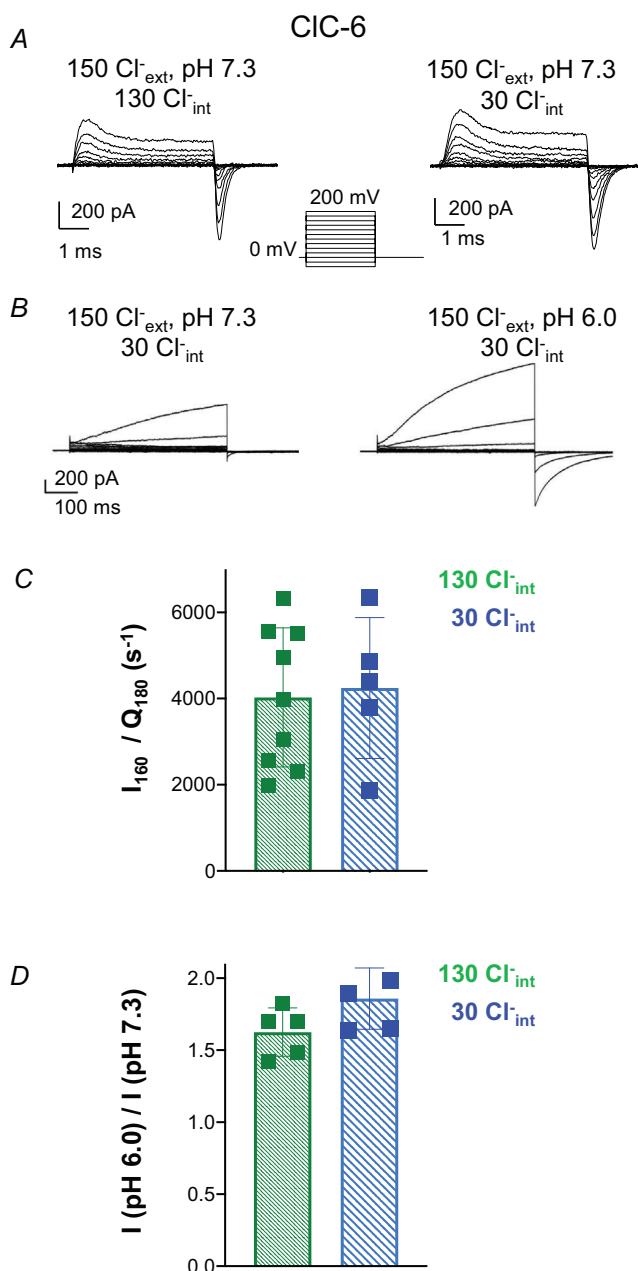
### Lowering extracellular $\text{Cl}^-$ reduces outward current mediated by CIC-6

Figure 1B shows examples of CIC-6 transport currents recorded in solutions at two different  $\text{pH}_{\text{ext}}$  values (7.3 and 6) and extracellular  $\text{Cl}^-$  concentrations (150 mM and 10 mM). As previously noted by Zifarelli et al. (Zifarelli et al., 2022), acidic  $\text{pH}_{\text{ext}}$  enhanced CIC-6-mediated outward and tail currents (Fig. 1B, top). This contrasts starkly with the effect of low  $\text{pH}_{\text{ext}}$  on most other CLC transporters (Friedrich et al., 1999; Picollo & Pusch, 2005; Picollo et al., 2010). In general, other CLCs are inhibited by low extracellular  $\text{Cl}^-$ , so we were curious whether lowered extracellular  $\text{Cl}^-$  would produce an inverse effect of increasing CIC-6 activity, similar to the inverse effect of reducing extracellular pH. Instead, lowering extracellular  $\text{Cl}^-$  from 150 mM to 10 mM also almost completely abolished outward currents (inward  $\text{Cl}^-$  movement) under both neutral and acidic  $\text{pH}_{\text{ext}}$  conditions (Fig. 1B, bottom; Fig. 1C), consistent with previous observations on other CLC transporters. Thus, with regard to extracellular  $\text{Cl}^-$ , CIC-6 responds like most other CLCs.

### Does reduction of intracellular $\text{Cl}^-$ concentration, $[\text{Cl}^-]_{\text{int}}$ , change CIC-6 activity?

Notably, the standard intracellular whole cell recording solution, containing 130 mM  $\text{Cl}^-$ , does not approximate cytosolic  $\text{Cl}^-$  concentration. For example, depending on developmental stage,  $[\text{Cl}^-]_{\text{int}}$  can range between  $\sim 20$  and 50 mM in mouse neurons (Sulis Sato et al., 2017). To test whether  $[\text{Cl}^-]_{\text{int}}$  affects properties of CIC-6 mediated currents, we performed recordings with  $[\text{Cl}^-]_{\text{int}}$  reduced to 30 mM. Transient currents elicited by rapid 5 ms pulses (Protocol 1) were qualitatively similar to those previously measured with  $[\text{Cl}^-]_{\text{int}}$  at 130 mM (Fig. 2A; (Zifarelli et al., 2022)). These transient currents reflect charge movement within the transporter protein, similar to 'gating currents' of voltage-gated cation channels. While the physiological role of transient currents is unclear, they constitute a typical biophysical feature (Guzman et al., 2013; Pusch & Zifarelli, 2021; Smith & Lippiat, 2010; Zifarelli et al., 2012, 2022).

Furthermore, with  $[\text{Cl}^-]_{\text{int}}$  reduced to 30 mM, transport currents recorded in extracellular 150 mM  $\text{Cl}^-$ , pH 7.3 solutions (Fig. 2B, left) displayed voltage dependence comparable to the voltage dependence of currents measured with pipette solutions containing 130 mM  $\text{Cl}^-$  (Fig. 1B, left). This observation held for measurements conducted at  $\text{pH}_{\text{ext}}$  6 as well (compare Fig. 2B, right with Fig. 1B, right).



**Figure 2. Low  $[\text{Cl}^-]_{\text{int}}$  does not affect transient and transport currents of CIC-6**

A, using an intracellular solution containing 30 mM  $\text{Cl}^-$  (right trace), transient currents elicited by Protocol 1 (inset) resemble those obtained using intracellular solution containing 130 mM  $\text{Cl}^-$  (left trace), as previously described (Zifarelli et al., 2022). B shows effect of extracellular acidification on transport currents elicited by Protocol 2, measured in the cell shown in A. C is a comparison of  $I_{160}/Q_{180}$ , the ratio of the ionic current (measured at 160 mV) and the integrated transient charge (at 180 mV) at 130 mM versus this ratio measured at 30 mM  $[\text{Cl}^-]_{\text{int}}$ . D shows  $I_{\text{pH } 6.0}/I_{\text{pH } 7.3}$ , the ratio of current measured at 160 mV at pH 6 and that measured at pH 7.3, at 130 mM versus 30 mM  $[\text{Cl}^-]_{\text{int}}$ .

To quantify the effect of low  $[Cl^-]_{int}$  on transport currents, we assessed the following two parameters. First, we calculated the ratio of the transport current measured at 160 mV to the transient charge movement after a pulse to 180 mV ( $I_{160}/Q_{180}$ ). Assuming that charge movement is not affected strongly by  $[Cl^-]_{int}$ , this ratio serves as a proxy for transport activity (Zifarelli et al., 2022). Figure 2C shows the ratio is unaltered in low  $[Cl^-]_{int}$  ( $I_{160}/Q_{180} = (4.0 \pm 1.6) \times 10^3 \text{ s}^{-1}$  for  $[Cl^-]_{int} = 130 \text{ mM}$  ( $n = 9$ ) and  $I_{160}/Q_{180} = (4.2 \pm 1.6) \times 10^3 \text{ s}^{-1}$  for  $[Cl^-]_{int} = 30 \text{ mM}$  ( $n = 5$ ),  $P = 0.811$ , Students unpaired  $t$  test). Secondly, we quantified the impact of extracellular acidification to pH 6 under both Cl<sup>-</sup>-replete and low  $[Cl^-]_{int}$  conditions by calculating the ratio of the transport currents measured at 160 mV, pH 6 and at 160 mV, pH 7.3 ( $I_{pH 6.0}/I_{pH 7.3}$ ) (Fig. 2D). In 130 mM  $[Cl^-]_{int}$ , the ratio was  $1.6 \pm 0.17$  ( $n = 5$ ) whereas the ratio in 30 mM  $[Cl^-]_{int}$  was  $1.8 \pm 0.2$  ( $n = 5$ ), indicating no appreciable difference in activation by low  $pH_{ext}$  ( $P = 0.0906$ ). These observations suggest that ClC-6 activity is insensitive to  $[Cl^-]_{int}$  in the considered concentration range.

### ClC-7 activity is increased by lowering extracellular Cl<sup>-</sup>

In contrast to the effects of extracellular acidity on ClC-6, it is well-appreciated that low  $pH_{ext}$  inhibits outward ClC-7 currents (Fig. 3A, top) (Friedrich et al., 1999; Leisle et al., 2011; Picollo et al., 2010; Pusch & Zifarelli, 2021). We therefore measured the effects of low extracellular Cl<sup>-</sup> on ClC-7 currents (Fig. 3A, bottom). Surprisingly, at pH 7.3, a 15-fold reduction of extracellular Cl<sup>-</sup> (to 10 mM) rendered a disproportionately mild reduction in WT ClC-7 outward transport current. Moreover, low extracellular Cl<sup>-</sup> produced inward tail currents exceeding those obtained in 150 mM, Cl<sup>-</sup>-replete extracellular solution (compare left panels, Fig. 3A), signifying activation, rather than inhibition, by low extracellular Cl<sup>-</sup>. Figure 3B plots normalized, steady-state, ClC-7 currents at voltages ranging from 140 mV to -80 mV, in the presence of 150 mM and 10 mM extracellular Cl<sup>-</sup>, at both neutral and acidic  $pH_{ext}$ . For the experiment shown in Fig. 3A, at the same extracellular conditions, the inward tail-currents at -80 mV are shown as a function of conditioning pre-pulse potential (Fig. 3C). For each extracellular condition tested, fitting the respective  $I_{tail}-V$  plots to the Boltzmann relationship revealed their average  $V_{1/2}$  values (Fig. 3D). Compared to measurements of ClC-7 acquired in control extracellular solutions (150 mM Cl<sup>-</sup>, pH 7.3), reducing extracellular Cl<sup>-</sup> to 10 mM shifted  $V_{1/2}$  toward less positive voltages. Moreover, this leftward shift associated with reduction of extracellular Cl<sup>-</sup> persisted at pH 6.

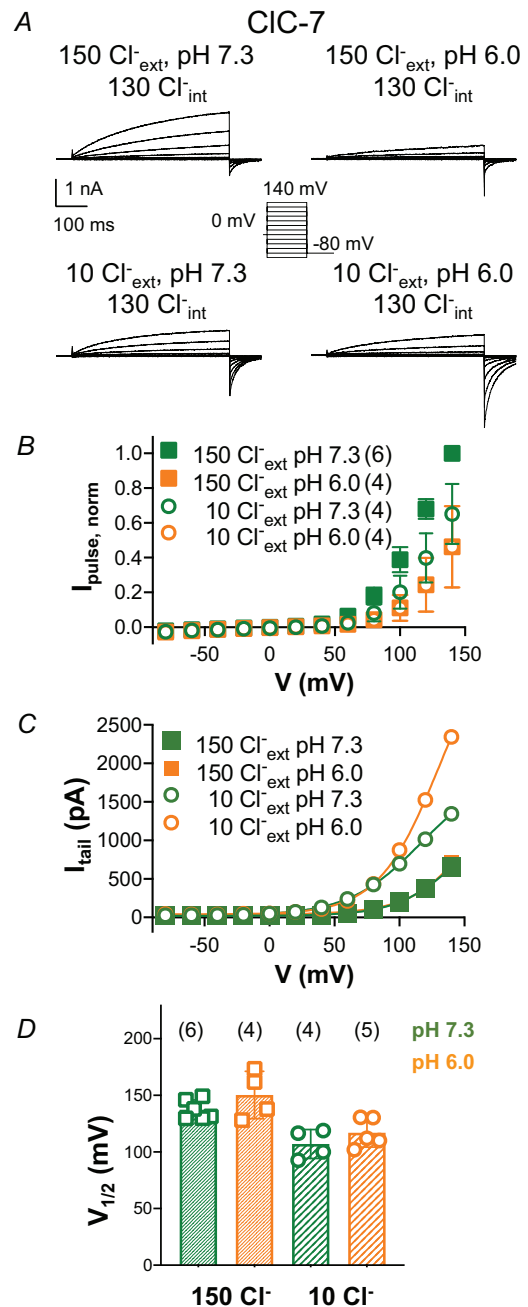


**Figure 3. ClC-7 is activated by low  $[Cl^-]_{ext}$**   
 A, typical transport currents elicited by Protocol 2 (see inset), measured in the same cell perfused with: 150 mM Cl<sup>-</sup>, pH 7.3 (top left); 150 mM Cl<sup>-</sup>, pH 6.0 (top right); 10 mM Cl<sup>-</sup>, pH 7.3 (lower left); 10 mM Cl<sup>-</sup>, pH 6.0 (lower right). B, normalized  $I-V$  relationship measured at the end of the test pulse. Points are mean normalized currents  $\pm$  SD obtained from the indicated number of cells. C, tail current analysis of recordings from the cell reported in A. Lines are fits of eqn (1). D, average values of  $V_{1/2}$  derived from fits with eqn (1) for data obtained in the indicated external solutions; mean  $\pm$  SD. At the control condition of 150 mM extracellular Cl<sup>-</sup>, pH 7.3,  $V_{1/2}$  was  $137.3 \pm 8.6$  mV. This shifted to  $107.1 \pm 12.7$  mV upon extracellular Cl<sup>-</sup> reduction (green bars;  $n = 6$  and  $n = 4$  for 150 mM and 10 mM extracellular Cl<sup>-</sup>, respectively;  $P = 0.0019$ ).

extracellular  $\text{Cl}^-$ , pH 6.0,  $V_{1/2}$  was  $150.3 \pm 20.9$  mV and shifted to  $117.0 \pm 12.8$  mV upon reduction to 10 mM extracellular  $\text{Cl}^-$  (orange bars;  $n = 4$  and  $n = 5$ , for 150 mM and 10 mM extracellular  $\text{Cl}^-$ ;  $P = 0.0212$ ).

### The combination of low extracellular $\text{Cl}^-$ and low $\text{pH}_{\text{ext}}$ activates CIC-7

The preceding data, showing the combined effect of low extracellular  $\text{Cl}^-$  and low  $\text{pH}_{\text{ext}}$  yields a  $V_{1/2}$  approximately 20 mV less positive than that measured for the  $\text{Cl}^-$ -replete, pH 7.3 control conditions. Hence, with the combination of both low extracellular  $\text{Cl}^-$  and low  $\text{pH}_{\text{ext}}$ , CIC-7 activation is preserved following highly depolarizing pre-pulses (Fig. 3C). To determine whether the increased inward tail currents reflect merely an altered driving force *versus* a change in the gating process, we investigated the kinetics of current changes in response to concentration jumps. The underlying assumption is that changes in driving-force are ‘immediately’ reflected in the current response, i.e. are only limited by the speed of perfusion, whereas gating processes might be associated with slower relaxations.

Starting from the standard 150 mM  $\text{Cl}^-$ , pH 7.3 extracellular solution, continuous bipolar pulses (Protocol 3; Fig. 4A) were applied and currents recorded whilst perfusing the bath rapidly with different extracellular solutions (Fig. 4B–D). Delivery of 150 mM  $\text{Cl}^-$ /pH 6 extracellular solution diminished outward currents, and the kinetics of the decline determined by fitting the current points at the peak of the depolarizing potential revealed a time constant,  $\tau$ , of 0.7 s (Fig. 4B). This value provides an upper limit for the perfusion exchange time. For the response to 10 mM extracellular  $\text{Cl}^-$ , fitting the change in inward currents at the peak of the hyperpolarizing pulse gave a  $\tau$  of 3.7 s (Fig. 4C). The combination of low  $\text{pH}_{\text{ext}}$  and low  $\text{Cl}^-$  yielded an even greater  $\tau$ , 5.3 s (Fig. 4D). These relatively large time constants demonstrate that activation by low extracellular  $\text{Cl}^-$  entails a seconds-long gating process that proceeds after full solutions exchange. Moreover, the persistence of both current activation and slow kinetics in the case of low  $\text{pH}_{\text{ext}}$  and extracellular  $\text{Cl}^-$  suggests that activation by the latter prevails over inhibition by low  $\text{pH}_{\text{ext}}$  in determining CIC-7 transport activity.

### CIC-7 activation by low extracellular $\text{Cl}^-$ persists at pH 5.0

Lysosomal luminal pH can acidify to  $\sim$ pH 4.5. At this pH, endogenous background acid-sensitive anion currents mediated by TMEM206 can obscure those carried by CIC-7. To evaluate effects at this more extreme

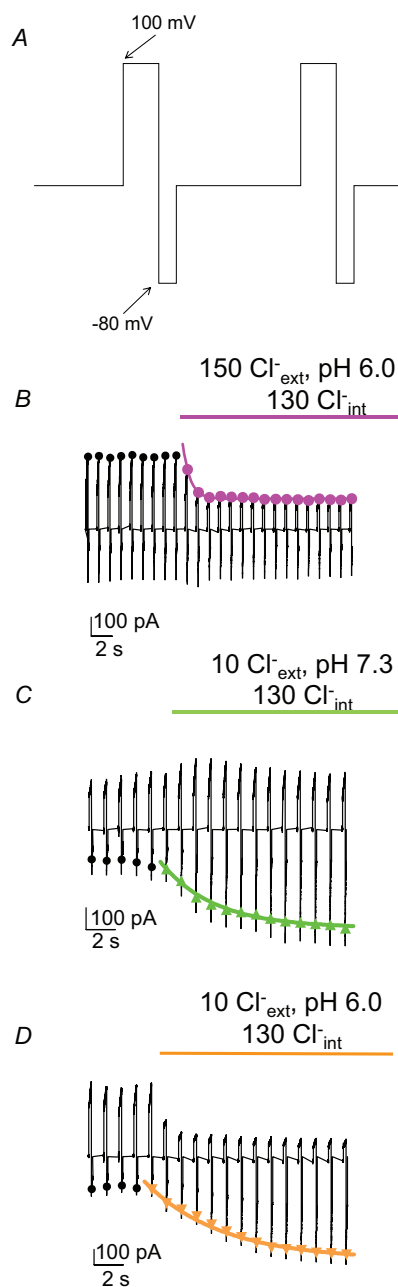


**Figure 4. Kinetics of activation of CIC-7 by low  $[\text{Cl}^-]_{\text{ext}}$**

A illustrates the pulse protocol used to monitor changes in activation upon rapid perfusion of different solutions. From a holding potential of 0 mV, a pulse waveform consisting of a 200 ms pulse to 100 mV, followed by 100 ms ‘tail’ pulse to  $-80$  mV, was delivered repeatedly at 1 Hz. Currents were measured at the end of the 100 mV pulse and at the beginning of the  $-80$  mV pulse. Initial conditions in all cases were 150 mM extracellular  $\text{Cl}^-$ , pH 7.3. B, depiction of a typical response upon perfusion of a solution containing 150 mM extracellular  $\text{Cl}^-$ , pH 6.0. Note that inward currents barely change, probably because the larger ‘driving force’ for  $\text{H}^+$  entry at pH 6 is partially offset by the reduction of transport activity via a ‘gating process’. The red line represents an exponential fit to outward currents indicated by the red dots, and yields a time constant of 0.7 s. This provides an upper limit for the time constant



of our perfusion system. *C*, typical response upon perfusion of a solution with 10 mM extracellular Cl<sup>-</sup>, pH 7.3. Note the lack of change in outward currents, probably due to partial compensation of the smaller 'driving force' for Cl<sup>-</sup> entry at 100 mV in 10 mM extracellular Cl<sup>-</sup> by the increased gating of transport activity. The green line is an exponential fit to the green symbols that yields a time constant of 3.7 s. *D*, typical response upon perfusion of a solution with 10 mM extracellular Cl<sup>-</sup>, pH 6. Note that outward currents change faster than inward currents, probably reflecting the reduced driving force for H<sup>+</sup> exit combined with the reduced driving force for Cl<sup>-</sup> entry. The orange line is an exponential fit to the orange symbols, having a time constant of 5.3 s.

condition, we expressed ClC-7 in acid-sensitive outwardly rectifying (ASOR)-deficient mammalian cells (HEK293 *TMEM206*<sup>-/-</sup>), thereby eliminating contributions of background acid-sensitive anion currents (Ullrich et al., 2019). Figure 5A shows typical currents in response to lowering pH<sub>ext</sub> to 5. As expected for ClC-7, acidic pH<sub>ext</sub> inhibits currents (Fig. 5C), revealing a depolarized  $V_{1/2}$  compared to the value obtained under control conditions (Fig. 5D, left). Lowering extracellular Cl<sup>-</sup> to 10 mM under conditions of neutral pH<sub>ext</sub> strongly activated inward tail currents (Fig. 5C), as reflected by the relatively less depolarized  $V_{1/2}$  compared to 150 mM Cl<sup>-</sup> control (Fig. 5D, green bars). The activating effect of lowering extracellular Cl<sup>-</sup> can be appreciated also by comparing  $V_{1/2}$  for lowered extracellular Cl<sup>-</sup> conditions at pH 5. Relative to the value obtained in 150 mM extracellular Cl<sup>-</sup>, pH 5, this remains markedly less depolarized (see Fig. 5D, red bars). Figure 5D (right) summarizes the effects of extracellular acidification under conditions of low extracellular Cl<sup>-</sup>. Here, the inhibitory effects of pH<sub>ext</sub> can be appreciated further; note the robust, positive shift ( $n = 4$ ,  $P = 0.0047$ ). These data support the notion that activation by low extracellular Cl<sup>-</sup> overrides inhibition by low pH<sub>ext</sub> in determining ClC-7 transport activity.

### Quantification of ClC-7 activation by lowered extracellular Cl<sup>-</sup>

To determine the extracellular [Cl<sup>-</sup>] required to activate ClC-7, we measured transport currents at 150, 40, 10 and 3 mM extracellular Cl<sup>-</sup> (Fig. 6A). Inward tail currents were discernibly larger at 40 mM (Fig. 6A). This can be appreciated as well in Fig. 6B, which plots the increase in peak inward tail current relative to the values for 150 mM extracellular Cl<sup>-</sup> ( $I_{X \text{ mM Cl}^-} / I_{150 \text{ mM Cl}^-}$ , indicated as  $I_{\text{norm}}$ ) as a function of the stimulating pulse potential. To quantify Cl<sup>-</sup> dependence, the  $I_{X \text{ mM Cl}^-} / I_{150 \text{ mM Cl}^-}$  ratios measured after a 1 s pre-pulse to 120 mV were calculated and plotted against the corresponding extracellular [Cl<sup>-</sup>] (Fig. 6C). The data points showing fractional current activity as a

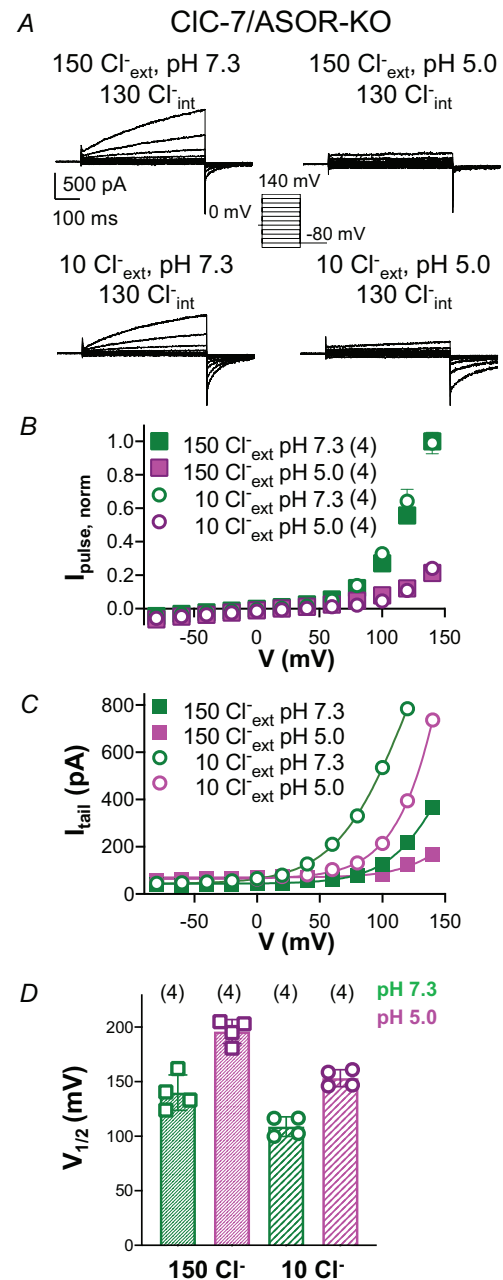


**Figure 5. Low [Cl<sup>-</sup>]<sub>ext</sub> activates ClC-7 expressed in ASOR-KO cells even at pH<sub>ext</sub> 5**

*A*, typical transport currents elicited by Protocol 2 (see inset), measured in the same cell in the indicated conditions. *B*, average normalized  $I$ - $V$  relationship measured at the end of the test pulse. *C*, tail current analysis of recordings from the cell reported in *A*. Lines are fits of eqn (1). *D*, average values of  $V_{1/2}$  derived from fits with eqn (1) in the various indicated conditions. For control 150 mM extracellular Cl<sup>-</sup>,  $V_{1/2}$  at pH<sub>ext</sub> 7.3 = 139.9 ± 16.2 mV (green bar, fine fill;  $n = 4$ ) whereas at pH<sub>ext</sub> 5.0,  $V_{1/2}$  = 195.9 ± 11.0 mV (magenta bar, fine fill;  $n = 4$ ). Comparison yields  $P = 0.00114$ . At 10 mM extracellular Cl<sup>-</sup>,  $V_{1/2}$  at pH<sub>ext</sub> 7.3 = 108.8 ± 8.9 mV (green bar, coarse fill;  $n = 4$ ); compared to control extracellular Cl<sup>-</sup> at neutral pH,  $P = 0.0153$ . At 10 mM extracellular Cl<sup>-</sup>, pH 5.0,  $V_{1/2}$  = 153.2 ± 7.8 mV (magenta bar, coarse fill;  $n = 4$ ); compared to  $V_{1/2}$  for 10 mM extracellular Cl<sup>-</sup>, pH 7.3,  $P = 0.0047$ . Relative to

$V_{1/2}$  measured for 150 mM extracellular  $\text{Cl}^-$  (magenta bars, fine fill), pH 5.0,  $P = 0.000929$ .

function of extracellular  $\text{Cl}^-$  were fitted with eqn (2b), yielding an apparent  $K_D$  value of 62 mM (Fig 6C).

### Does intracellular $\text{Cl}^-$ influence low extracellular $\text{Cl}^-$ activation of CIC-7?

To test the effect of physiological  $[\text{Cl}^-]_{\text{int}}$  on activation by extracellular  $\text{Cl}^-$  reduction, we performed whole cell recordings using a pipette solution containing 30 mM  $\text{Cl}^-$ . Figure 6D depicts typical traces obtained in 150 and 10 mM extracellular  $\text{Cl}^-$ , but under conditions of lowered intracellular  $\text{Cl}^-$ . Note their overall resemblance to those obtained in  $\text{Cl}^-$ -replete intracellular solution (compare to corresponding panels in Fig. 6A, top and bottom left). The potentiating effect of 10 mM extracellular  $\text{Cl}^-$  on CIC-7 persisted, even at reduced  $[\text{Cl}^-]_{\text{int}}$ . To quantify the impact of reducing extracellular  $\text{Cl}^-$  from 150 mM to 10 mM, we calculated the ratio of outward currents measured at the end of the 120 mV test pulse ( $I_{(10 \text{ Cl}_{\text{ext}})}/I_{(150 \text{ Cl}_{\text{ext}})}$ ), and compared the values for both intracellular  $\text{Cl}^-$  conditions (Fig. 6E). For measurements performed in 30 mM  $\text{Cl}^-_{\text{int}}$ , this ratio was  $0.710 \pm 0.017$  ( $n = 4$ ) whereas for 130 mM intracellular  $\text{Cl}^-$ , this was  $0.615 \pm 0.069$  ( $n = 6$ ). These findings suggest slight enhancement by 10 mM extracellular  $\text{Cl}^-$  under conditions of low intracellular  $\text{Cl}^-$  (i.e. cytosolic  $\text{Cl}^-$ ) ( $P = 0.0299$ , Student's  $t$  test), possibly via crosstalk through pore occupancy and the gating glutamate.

### Studies to probe whether CIC-6 GoF mutant alters dependence on extracellular $\text{Cl}^-$

In CIC-6, Tyr<sup>553</sup> localizes close to the dimer interface, at the luminal aspect of the transporter, corresponding to the extracellular side in plasma membrane expressing transporters (Fig. 1A). Its mutation to cysteine results in GoF due to a leftward voltage shift in transporter activation, thereby contributing to early-onset human neurodegenerative disease (Polovitskaya et al., 2020; Zifarelli et al., 2022). Polovitskaya and colleagues (Polovitskaya et al., 2020) suggested that CIC-6<sup>Y553C</sup> might exert its effects via cysteine bridging with a neighbouring cysteine (either Cys<sup>319</sup> or Cys<sup>326</sup>) in the same subunit. Compared to WT CIC-6, acidic pH<sub>ext</sub> activated CIC-6<sup>Y553C</sup> transport currents to a lesser extent (Zifarelli et al., 2022). Figure 7A shows typical current traces resulting from lowering extracellular  $\text{Cl}^-$ , pH, and the combination of the two conditions. Similar

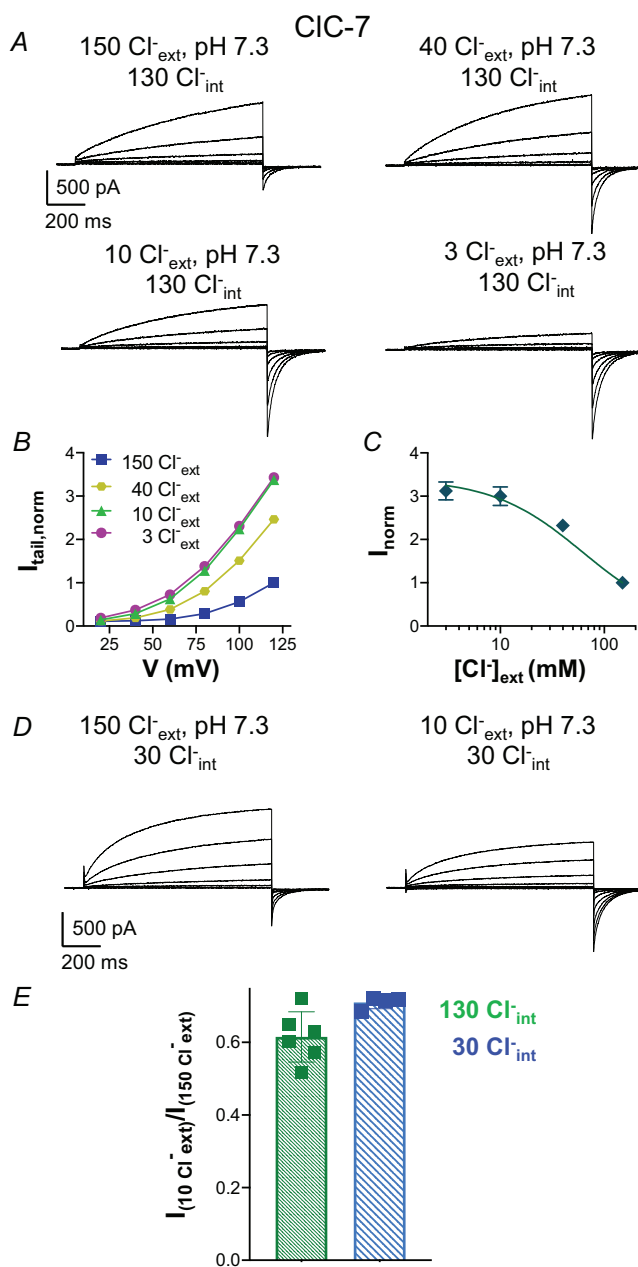


**Figure 6.  $[\text{Cl}^-]_{\text{ext}}$  dependence of CIC-7 and effect of reducing  $[\text{Cl}^-]_{\text{int}}$**

A, typical transport currents elicited by Protocol 2 (with pulse length of 1 s), measured in the same cell at the indicated range of  $[\text{Cl}^-]_{\text{ext}}$ . B shows the normalized  $I$ - $V$  relationships of the same cell depicted in A measured at the end of the test pulse. C plots the  $[\text{Cl}^-]_{\text{ext}}$  dependence of normalized currents measured at the end of the 120 mV test pulse. The line shows the fit obtained using eqn (2b), resulting in an apparent  $\text{EC}_{50}$  of 62 mM. D, typical transport currents elicited by Protocol 2, obtained using an intracellular solution containing 30 mM  $\text{Cl}^-$  from the same cell, under the indicated extracellular conditions. E shows a comparison of  $I_{(10 \text{ Cl}_{\text{ext}})}/I_{(150 \text{ Cl}_{\text{ext}})}$ , the ratio of current measured at 120 mV in 10 mM extracellular  $\text{Cl}^-$  against that measured in 150 mM extracellular  $\text{Cl}^-$ , under conditions of full and low  $[\text{Cl}^-]_{\text{int}}$  (130 mM and 30 mM).

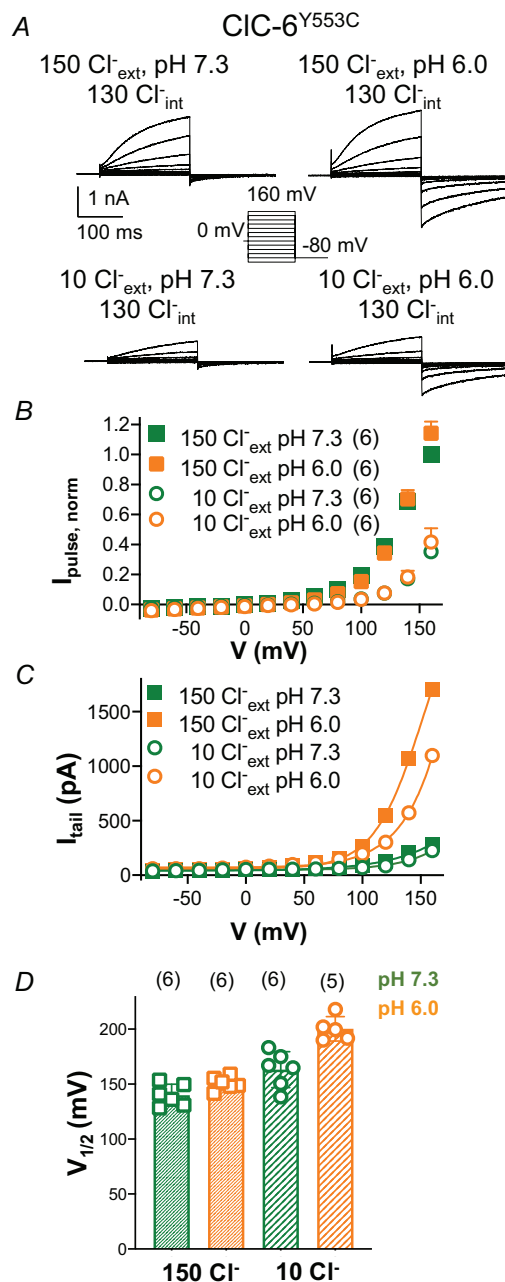


**Figure 7. Dependence of CIC-6<sup>Y553C</sup> on low [Cl<sup>-</sup>]<sub>ext</sub>**

A, typical transport currents elicited by Protocol 2 (see inset), measured in the same cell at the indicated conditions. B, average normalized  $I$ - $V$  relationship measured at the end of the test pulse from the indicated number of cells. C, tail current analysis of recordings from the cell reported in A. Lines are fits of eqn (1). D, average values of  $V_{1/2}$  are derived from fits with eqn (1) in the various indicated conditions. In control solution, (150 mM extracellular Cl<sup>-</sup>, pH 7.3)  $V_{1/2} = 139.9 \pm 10.0$  mV and with reduction of [Cl<sup>-</sup>]<sub>ext</sub> to 10 mM, depolarized to  $163.2 \pm 6.6$  mV (green bars;  $n = 6$  for both conditions;  $P = 0.0140$ ). Reducing Cl<sup>-</sup>-replete solution pH to 6.0 depolarized  $V_{1/2}$  to  $150.7 \pm 6.1$  mV ( $n = 6$ ; compared to control solution conditions,  $P = 0.0482$ ). Simultaneous reduction of both pH<sub>ext</sub> and extracellular Cl<sup>-</sup> markedly depolarized  $V_{1/2}$  to  $200.2 \pm 10.9$  mV ( $n = 5$ , compared to control  $P < 0.0001$ ).

to WT CIC-6, pH<sub>ext</sub> 6 strongly increased inward tail currents. Although 10 mM extracellular Cl<sup>-</sup> reduced tail currents, the effect was incomplete compared to that observed for WT CIC-6. Also in contrast to WT CIC-6, CIC-6<sup>Y553C</sup> tail current activation by low pH<sub>ext</sub> persisted when combined with low extracellular Cl<sup>-</sup> challenge (compare Fig. 1B with Fig. 7A, right panels). Figure 7B–D summarizes average, normalized  $I_{ss}$ - $V$  relationships, provides an example of the Boltzmann fits, and plots average  $V_{1/2}$  values determined from the fits. At pH 7.3, reduction of extracellular Cl<sup>-</sup> shifted  $V_{1/2}$  rightward, towards more depolarized potentials. Simultaneous reduction of pH<sub>ext</sub> and extracellular Cl<sup>-</sup> did not mitigate – and indeed enhanced – the rightward shift in  $V_{1/2}$ . Note that the extremely positive voltages required for WT CIC-6 activation prohibited similar quantitative estimates of its gating parameters. Nonetheless, assuming that the CIC-6<sup>Y553C</sup> mutant qualitatively reflects the Cl<sup>-</sup> dependence of WT CIC-6, we can conclude that low extracellular Cl<sup>-</sup> shifts gating significantly to more positive voltages, opposite to what was observed for CIC-7.

#### Studies of the corresponding CIC-7<sup>Y577C</sup> mutant rules out a hypothesized mechanism for CIC-6<sup>Y553C</sup> GoF

Polovitskaya et al. (2020) proposed CIC-6<sup>Y553C</sup> GoF might result from intra-monomeric reactivity of Cys<sup>553</sup> with Cys<sup>319</sup> or Cys<sup>326</sup>. We asked whether the corresponding CIC-7 mutation, CIC-7<sup>Y577C</sup> (Fig. 1A), similarly activates transporter gating. Because CIC-7 lacks potential partner cysteines at positions corresponding to either Cys<sup>319</sup> or Cys<sup>326</sup> of CIC-6, the mechanism proposed by Polovitskaya et al. (2020) predicts that CIC-7<sup>Y577C</sup> would not display GoF. Indeed, overexpression of CIC-7<sup>Y577C</sup> did not produce enlarged, distended vacuoles, in contrast to cells overexpressing CIC-6<sup>Y553C</sup> (Polovitskaya et al., 2020).

Surprisingly however, as shown in Fig. 8A, CIC-7<sup>Y577C</sup> expression displayed strongly activated currents compared to WT CIC-7, and panels B–D depict the corresponding normalized  $I_{ss}$ - $V$  plots and Boltzmann analyses. Similar to WT CIC-7 in Cl<sup>-</sup>-replete extracellular conditions, CIC-7<sup>Y577C</sup> is inhibited by low pH<sub>ext</sub>; note the much smaller outward currents (Fig. 8A, top right). Note also the more positive  $V_{1/2}$  values at more acidic pH (Fig. 8D, left).

At pH 7.3, lowering extracellular Cl<sup>-</sup> to 10 mM activates CIC-7<sup>Y577C</sup> and leads to a dramatic acceleration of activation kinetics, yielding a markedly less positive  $V_{1/2}$  than that obtained in control conditions (150 mM extracellular Cl<sup>-</sup>, pH 7.3). In addition, in low extracellular Cl<sup>-</sup> the transporter is active even at the holding potential of 0 mV, as can be seen from the deactivating currents when stepping to negative voltages (Fig. 8A, bottom left). This behaviour is even more dramatic with the

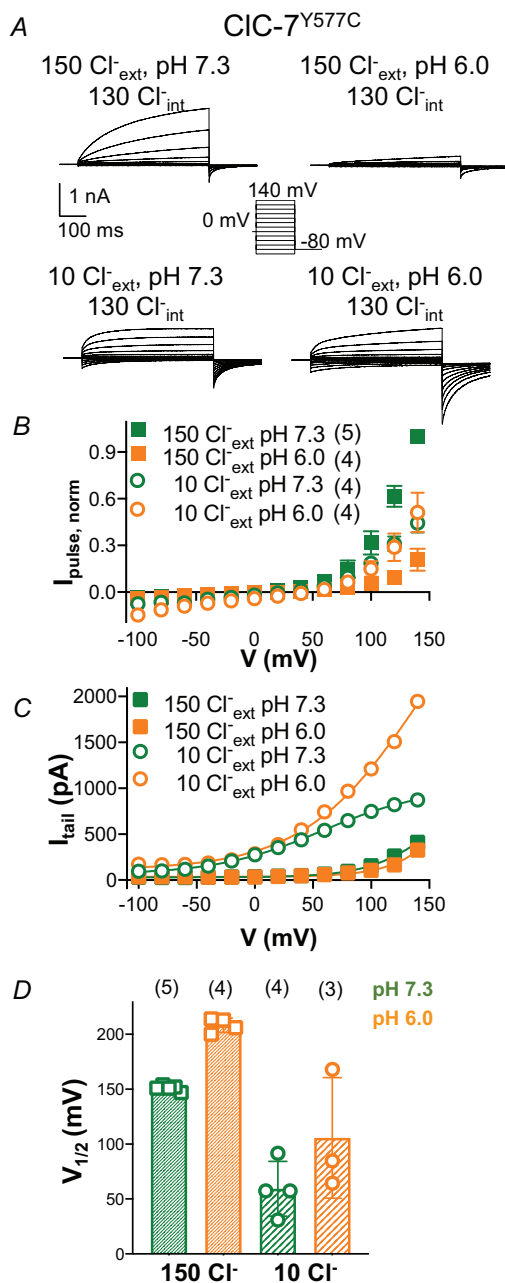


**Figure 8. Dependence of CIC-7<sup>Y577C</sup> on low [Cl<sup>-</sup>]<sub>ext</sub>**

A, typical transport currents elicited by Protocol 2 (see also inset), measured in the same cell in the indicated conditions. B, average normalized  $I-V$  relationship measured at the end of the test pulse. C, tail current analysis of recordings from the cell shown in A. Lines are fits of eqn (1). D, average values of  $V_{1/2}$  derived from fits with eqn (1) in the various indicated conditions. From the left: In control, 150 mM extracellular  $Cl^-$ , pH 7.3 recording solution,  $V_{1/2} = 148.5 \pm 6.3$  mV whereas records obtained in 150 mM extracellular  $Cl^-$ , pH 6 solution gave  $V_{1/2} = 208 \pm 6.5$  mV ( $n = 5$  and 4, respectively;  $P < 0.0001$ ). Lowering extracellular  $Cl^-$  to 10 mM, maintaining a pH of 7.3, yields  $V_{1/2}$  of  $59 \pm 24$  mV ( $n = 4$ ;  $P < 0.0001$ , compared to  $V_{1/2}$  in 150 mM extracellular  $Cl^-$ , pH 7.3). In 10 mM extracellular  $Cl^-$ , pH 6.0,  $V_{1/2} = 105 \pm 54$  mV ( $n = 3$ ; comparison between the low  $Cl^-$  groups gives  $P = 0.187$ ).

combination of low extracellular  $Cl^-$  and pH 6; in this case the transporter is almost constitutively active (Fig. 8A, bottom right). Although low  $pH_{ext}$  appears to shift  $V_{1/2}$  to more positive potentials (Fig. 8D, right), the present findings do not achieve significance.

### Activation by low extracellular $Cl^-$ is conserved in a CIC-7 variant with disrupted PI(3,5)P<sub>2</sub> inhibition

A human disease-associated CIC-7 variant, CIC-7<sup>Y715C</sup>, localizes to the cytosolic aspect of the transporter and evidently confers GoF by disrupting a binding site critical for tonic PI(3,5)P<sub>2</sub> inhibition (Leray et al., 2022) (Fig. 1A). This provided an opportunity to study whether GoF conferred by intracellular disruption of this site affects activation by low extracellular  $Cl^-$ . To this end, we evaluated the effects of lowering bath  $[Cl^-]$ , lowering  $pH_{ext}$ , and the combination of both on rat CIC-7<sup>Y713C</sup> transport currents. Figure 9 shows typical current responses, as well as the normalized  $I_{ss}-V$  relationships and Boltzmann plots for measurements obtained under these conditions. Reducing  $pH_{ext}$  from 7.3 to 6.0 under  $Cl^-$ -replete conditions depolarized  $V_{1/2}$  only slightly, proportionally similar to the effect on WT CLC-7 (~10%; compare Fig. 9D, left with Fig. 3D, left). In contrast, at neutral  $pH_{ext}$ , lowering extracellular  $Cl^-$  activated transport strongly, as reflected in a marked shift of  $V_{1/2}$  to less depolarized potentials (Fig. 9D; compare green bars). The relatively hyperpolarized  $V_{1/2}$  produced by low extracellular  $Cl^-$  conditions was less marked when  $pH_{ext}$  was lowered to 6.0. This suggests that acidification blunts the activating effect of low extracellular  $Cl^-$  on CIC-7<sup>Y713C</sup>. Nonetheless, compared to control conditions,  $V_{1/2}$  measured under low extracellular  $Cl^-$ , acid conditions remained left-shifted.

### CIC-6<sup>Y781C</sup> responsiveness to low $pH_{ext}$ and extracellular $Cl^-$

In the context of CLC-6, the corresponding mutant, CIC-6<sup>Y781C</sup> (Fig. 1A), qualitatively behaved like WT CLC-6 (compare recordings Fig. 1B with Fig. 10A). Activation by low  $pH_{ext}$  remained, whereas both extracellular  $Cl^-$  reduction and the combination of both low  $pH_{ext}$  and extracellular  $Cl^-$  eliminated current fully. Figure 10B summarizes the average, normalized  $I_{ss}-V$  relationships for CIC-6<sup>Y781C</sup> under the conditions tested, and Fig. 10C plots  $I_{tail}-V$ . Yet again, the extreme depolarization required for transporter activation precludes reliable extraction of Boltzmann fit parameters for the mutant.

Although the current-density did not differ between WT CLC-6 and CIC-6<sup>Y781C</sup> (Fig. 10D) the mutation significantly accelerated kinetics of activation at positive



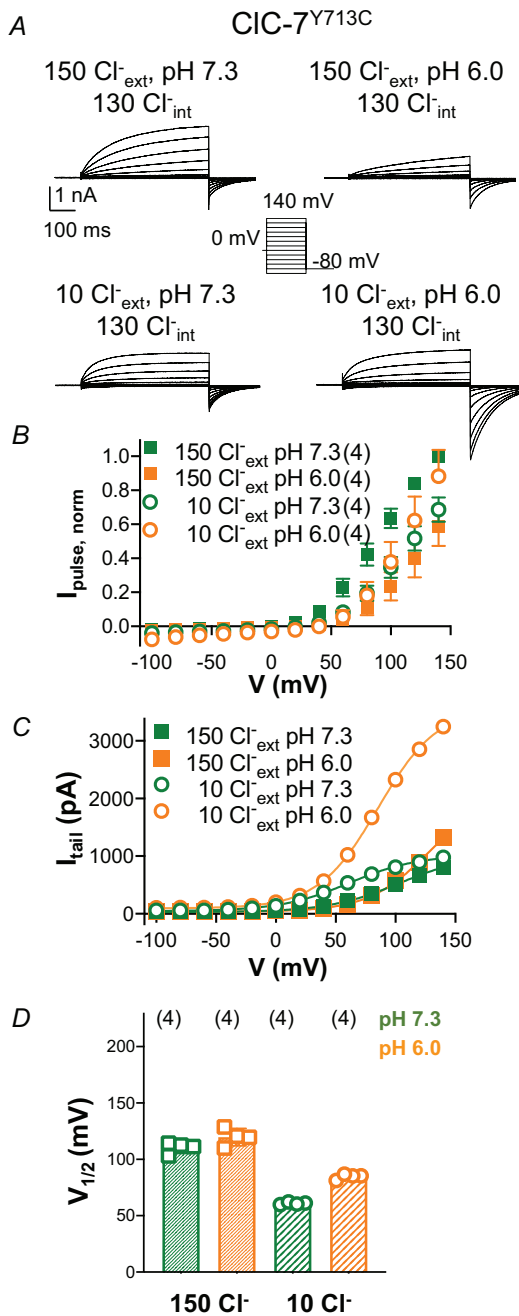


**Figure 9. Dependence of ClC-7<sup>Y713C</sup> on low [Cl<sup>-</sup>]<sub>ext</sub>**

A, typical transport currents elicited by Protocol 2 (see also inset), measured in the same cell in the indicated conditions. B, average normalized  $I$ - $V$  relationship measured at the end of the test pulse. C, tail current analysis of recordings obtained from the cell reported in A. Lines are fits of eqn (1). D, average values of  $V_{1/2}$  derived from fits with eqn (1) in the various indicated conditions. For control conditions (150 mM extracellular Cl<sup>-</sup>, pH 7.3),  $V_{1/2}$  was  $110 \pm 5$  mV, and reduction of pH to 6.0 produced  $V_{1/2}$  of  $120 \pm 8$  mV;  $n = 4$  for both conditions;  $P = 0.205$ . In 10 mM extracellular Cl<sup>-</sup>, pH 7.3,  $V_{1/2} = 61 \pm 1$  mV ( $n = 4$ ;  $P = 0.0003$  compared to  $V_{1/2}$  obtained under control conditions). For 10 mM extracellular Cl<sup>-</sup>, pH 6.0,  $V_{1/2} = 84 \pm 2.4$  mV ( $n = 4$ ;  $P = 0.0002$  compared to  $V_{1/2}$  obtained in low Cl<sup>-</sup>, neutral pH, and  $P = 0.0028$  compared to control conditions).

voltages, as well as its deactivation at  $-80$  mV (Fig. 10E), under both neutral and acidic pH conditions. This effect mirrors the properties of the ClC-7<sup>Y715C</sup> mutation that exhibited a roughly 2-fold acceleration of activation kinetics (Leray et al., 2022). Thus, the ClC-6<sup>Y781C</sup> mutation appears to activate transport in a manner qualitatively similar to the corresponding mutation in ClC-7.

### Studies testing effects of low extracellular Cl<sup>-</sup> on a 'fast' osteopetrosis variant

Several inherited variants of ClC-7 associated with autosomal dominant osteopetrosis exhibit an apparently paradoxical acceleration of activation kinetics of currents (Di Zanni et al., 2021; Leisle et al., 2011). For example, hClC-7<sup>R762Q</sup> (Fig. 1A) exhibits dramatic acceleration of gating kinetics and apparently unimpaired subcellular targeting when over-expressed in HeLa cells (Kornak et al., 2001; Leisle et al., 2011). These observations confound facile explanations for loss of function (LoF) in the aetiology of osteopetrosis. Is ClC-7<sup>R762Q</sup> activation by extracellular Cl<sup>-</sup> intact? We pursued this question using the corresponding rat point mutant, ClC-7<sup>R760Q</sup>. Figure 11 shows examples of currents carried by ClC-7<sup>R760Q</sup> under control conditions, as well as in low pH, in 10 mM extracellular Cl<sup>-</sup>. Under Cl<sup>-</sup>-replete conditions, lowering pH<sub>ext</sub> inhibited outward ClC-7<sup>R760Q</sup> transport currents, consistent with wild-type ClC-7 (Fig. 11A). Moreover, Boltzmann fit of tail current  $I$ - $V$  curves revealed that reduction to pH 6.0 shifted  $V_{1/2}$  in the positive direction (Fig. 11D, left). Surprisingly, activation by low extracellular Cl<sup>-</sup> appeared to be absent at the level of inward tail currents. In fact, reducing extracellular Cl<sup>-</sup> to 10 mM at neutral pH<sub>ext</sub> showed no effective change in mean  $V_{1/2}$  (Fig. 11D, compare green bars). Nevertheless, reducing extracellular Cl<sup>-</sup> and lowering pH<sub>ext</sub> to 6.0 significantly left-shifted  $V_{1/2}$  compared to the value obtained by lowering pH<sub>ext</sub> under Cl<sup>-</sup>-replete conditions (compare orange bars). This suggests that under acidic conditions, low Cl<sup>-</sup> can still partially activate the transporter.

While these differences point to a complex effect of the mutation on Cl<sup>-</sup> and pH dependence, they could determine the pathophysiological outcome.

### Discussion

We discovered that exposure to low extracellular Cl<sup>-</sup> strongly activates plasma membrane-expressed, lysosomal ClC-7/Ostm1 transporters. Activation persisted under acidic extracellular conditions as low as pH 5, a condition that strongly inhibits ClC-7 in Cl<sup>-</sup>-replete conditions (Leisle et al., 2011). Interestingly, we found that low extracellular Cl<sup>-</sup> strongly inhibited the closely

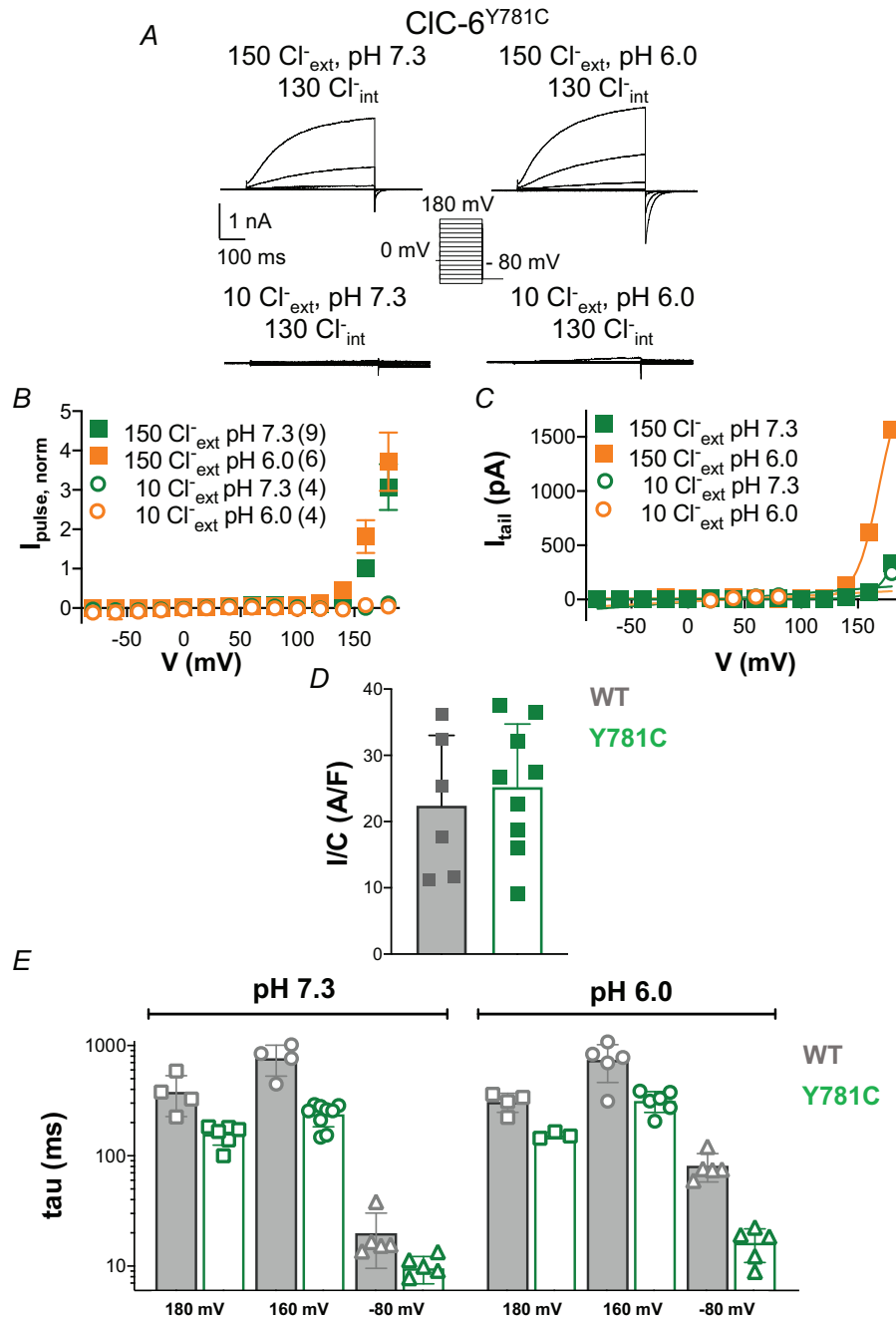


**Figure 10. Properties of CIC-6<sup>Y781C</sup>**

A, typical transport currents elicited by Protocol 2 (see also inset), measured in the same cell in the indicated conditions. B, average normalized  $I$ - $V$  relationship measured at the end of the test pulse. C, tail current analysis of recordings obtained from the cell reported in A. Lines are fits of eqn (1). D, current density (i.e. current amplitude divided by cell capacitance,  $I/C$ ) measured at 160 mV in pH 7.3 for WT CIC-6 was  $22.4 \pm 10.6$  A/F ( $n = 6$  cells). For CIC-6<sup>Y781C</sup>, this was  $25.2 \pm 9.5$  A/F ( $n = 9$  cells). Comparison of  $I/C$  for the two groups yields  $P = 0.603$ . E, activation and deactivation time constants of WT CIC-6 and CIC-6<sup>Y781C</sup> currents, measured for the indicated conditions (pH 7.3 and 6.0) by fitting a single exponential function to the current relaxations after voltage steps ( $V_{\text{hold}} = 180, 160,$  and  $-80$  mV). Under neutral pH conditions (pH 7.3), at 180 mV,  $\tau = 379 \pm 152$  s ( $n = 4$ ) for WT CIC-6 and  $157 \pm 32$  s ( $n = 6$ ) for CIC-6<sup>Y781C</sup> ( $n = 4$  and 6, respectively;  $P = 0.00736$ ). At 160 mV, pH 7.3,  $\tau = 767 \pm 238$  s for WT CIC-6 and  $238 \pm 55$  s for CIC-6<sup>Y781C</sup> ( $n = 4$  for WT, and  $n = 9$  for CIC-6<sup>Y781C</sup>,  $P = 3.77 \times 10^{-5}$ ). At  $-80$  mV, pH 7.3, for WT CIC-6  $\tau = 19.9 \pm 10.3$  s; for CIC-6<sup>Y781C</sup> it was  $9.6 \pm 2.6$  s ( $n = 5$  and  $n = 6$ , respectively;  $P = 0.0415$ ). Under acidic conditions (pH 6.0), at 180 mV,  $\tau = 308 \pm 60$  s for WT CIC-6 and  $153 \pm 11$  s for CIC-6<sup>Y781C</sup> ( $n = 4$  and 3, respectively;  $P = 0.00786$ ). Fits obtained from WT CIC-6 and

ClC-6<sup>Y781C</sup> currents measured at 160 mV, pH 6.0 yielded  $\tau = 308 \pm 61$  s and  $153 \pm 11$  s, respectively ( $n = 5$  for WT and  $n = 6$  for ClC-6<sup>Y781C</sup>;  $P = 0.00525$ ). For  $-80$  mV, pH 6,  $\tau = 81.2 \pm 23.3$  s for WT ClC-6 and  $16.2 \pm 5.5$  s for ClC-6<sup>Y781C</sup>, (for both,  $n = 5$ ;  $P = 0.000299$ ).

related ClC-6, which requires large positive voltages for activity (Zifarelli et al., 2022). In stark contrast to ClC-7, ClC-6 is more active in low pH<sub>ext</sub> (Zifarelli et al., 2022). However, in combination with low Cl<sup>-</sup>, its inhibition by low Cl<sup>-</sup> prevailed, such that pulses up to 180 mV failed to evoke measurable transport currents.

These findings carry potential physiological relevance. One may wonder whether the large positive voltages needed to activate ClC-6 and ClC-7 can be achieved in the physiological setting, given reports of lysosomal membrane potential within the range of  $-20$  to  $-40$  mV (Xu & Ren, 2015). This conundrum has been previously discussed in depth (Jentsch & Pusch, 2018; Zifarelli et al., 2022). At this time, we firmly believe that the best argument supporting physiological relevance for the strong voltage dependence of both transporters rests in the fact that GoF mutations disrupting the voltage dependence give rise to severe neurodegeneration (Nicoli et al., 2019; Polovitskaya et al., 2020). Our finding of an opposite dependence of ClC-6 and ClC-7 on the transported substrates – Cl<sup>-</sup> ions and protons – strongly suggest that they play non-overlapping functional roles. Very little is known about the physiological role of ClC-6. Its knock-out in mice leads to mild neuronal ceroid lipofuscinosis (NCL) (Poët et al., 2006), and a LoF mutation, ClC-6<sup>V580M</sup>, has been associated with Kufs' disease, a late onset human NCL disease (Poët et al., 2006; Zifarelli et al., 2022). These observations suggest a role for ClC-6 in delivery of material from late-endosomes to lysosomes. More recently, the mutation ClC-6<sup>Y553C</sup> was found to cause early-onset neurodegeneration (Polovitskaya et al., 2020). Functionally, ClC-6<sup>Y553C</sup> activates at less extreme positive voltages than WT ClC-6, and displays much faster gating kinetics, suggesting a GoF effect (Polovitskaya et al., 2020; Zifarelli et al., 2022). This tyrosine residue is conserved in ClC-7, specifically as Y577 in the rat clone. Our findings reveal that ClC-7<sup>Y577C</sup> produces currents consistent with GoF, exhibiting accelerated kinetics and dramatic activation by low extracellular chloride. This finding is important, as one possible mechanism for ClC-6<sup>Y553C</sup> GoF entertained the notion that it might result from intra-monomeric cysteine bridging (Polovitskaya et al., 2020). Because ClC-7 does not harbour the putative partner cysteines in the appropriate region, bridging cannot explain GoF displayed by ClC-7<sup>Y577C</sup>. Although our findings do not fully rule this out as a mechanism for ClC-6<sup>Y553C</sup> GoF, they do weaken the case for cysteine bridging. Nonetheless, our finding that ClC-7<sup>Y577C</sup> results in similar

transport activation as the corresponding ClC-6<sup>Y553C</sup> mutant further underscores conserved voltage-dependent activation mechanisms between ClC-6 and ClC-7, despite their differing responses to pH<sub>ext</sub> and extracellular Cl<sup>-</sup>. Importantly, both GoF mutants, ClC-6<sup>Y553C</sup> and ClC-7<sup>Y577C</sup>, retained the Cl<sup>-</sup> dependence of the respective WT. In fact, mutant ClC-7<sup>Y577C</sup> showed a largely reduced voltage dependence in 10 mM Cl<sup>-</sup> and pH 6 with a significant constitutive activity. Regarding the physiological roles of ClC-6 versus ClC-7, our finding that overexpression of ClC-7<sup>Y577C</sup> does not cause vacuolation of cells, as does the expression of ClC-6<sup>Y553C</sup> (Polovitskaya et al., 2020), provides further evidence that the two transporters have non-overlapping physiological roles.

The activation of ClC-7 by low extracellular/luminal Cl<sup>-</sup> suggests an important role in lysosomal biology. Two major hypotheses regarding its function are currently debated. The first hypothesis proposes that ClC-7 transport provides counter charge to the electrogenic H<sup>+</sup>-ATPase, allowing efficient acidification of lysosomes and resorption lacunae of osteoclasts (Graves et al., 2008). This conclusion mainly arose from observations of reduced lysosomal acidification in *CLCN7*-siRNA knockdown cells (Graves et al., 2008). Recently, Nicoli et al. (2019) described ClC-7<sup>Y715C</sup>, a GoF variant associated with delayed myelination and development, organomegaly and hypopigmentation. Lysosomes of cells of patients carrying this variant were more acidic than control cells, suggesting that increased ClC-7 activity leads to lysosomal hyperacidification (Nicoli et al., 2019), providing further support for this hypothesis. PI(3,5)P<sub>2</sub> inhibition of WT ClC-7 was abolished in ClC-7<sup>Y715C</sup> (Leray et al., 2022), thus suggesting a mechanism whereby PI(3,5)P<sub>2</sub> partially inhibits ClC-7 activity tonically, limiting lysosomal acidity. Mutation of Y715 thus releases inhibition, resulting in hyperacidification. Although the mutant loses sensitivity to PI(3,5)P<sub>2</sub> (Leray et al., 2022), our findings demonstrate that it is still activated by low extracellular Cl<sup>-</sup>. This suggests that PI(3,5)P<sub>2</sub> and luminal Cl<sup>-</sup> affect ClC-7 gating by different mechanisms. The relevant tyrosine is conserved in ClC-6. Upon expression of the corresponding mutant, ClC-6<sup>Y781C</sup>, we found that gating kinetics were significantly accelerated, similar to what is observed in ClC-7<sup>Y715C</sup> (Leray et al., 2022), and in agreement with a similar GoF effect, suggesting a similar role of the cytoplasmic domains in ClC-6 and ClC-7 in controlling transporter gating. Further studies are necessary to investigate the possible regulation of ClC-6 by phosphatidylinositol phosphates and the involvement of Y781 in this process.

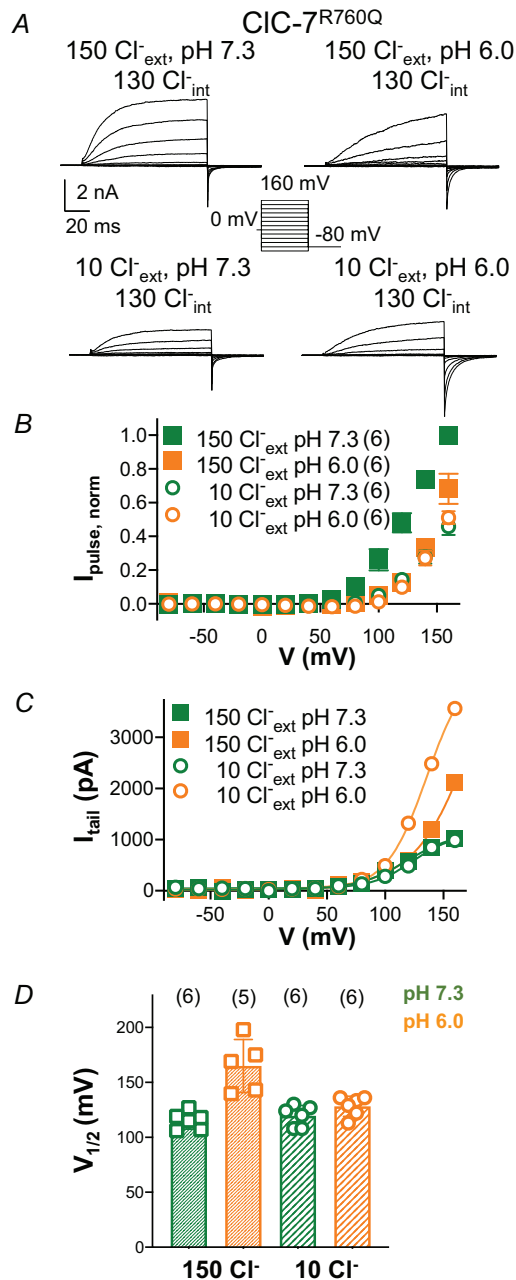


**Figure 11.** Effects of low  $[Cl^-]_{ext}$  on  $CIC-7^{R760Q}$

A, typical transport currents elicited by Protocol 2 (see inset), measured in the same cell at the indicated conditions. Note scale bars showing the shorter pulse duration compared to the other measurements. B, average normalized  $I-V$  relationship measured at the end of the test pulse for the indicated number of cells. C, tail current analysis of recordings from the cell reported in A. Lines are fits of eqn (1). D, average values of  $V_{1/2}$  derived from fits with eqn (1) in the various indicated conditions. From the left, in 150 mM extracellular  $Cl^-$ , at pH 7.3 (control),  $V_{1/2} = 115 \pm 7.8$  mV ( $n = 6$ ); at pH 6.0,  $V_{1/2} = 165 \pm 24$  mV ( $n = 5$ ). A comparison of these values yields  $P = 0.00100$ . In 10 mM extracellular  $Cl^-$ , at pH 7.3,  $V_{1/2} = 119 \pm 9$  mV ( $n = 6$ ), indicating no effective change from control conditions ( $P = 0.418$ ). In 10 mM extracellular  $Cl^-$ , pH 6.0,  $V_{1/2} = 128 \pm 9$  mV ( $n = 6$ ). Compared to 150 mM extracellular  $Cl^-$ , pH 6.0,  $P = 0.00709$ .

Contradicting an essential role for  $CIC-7$  in lysosomal acidification, lysosomal pH of cells derived from WT,  $CIC-7$  KO mice and  $Ostm1$  KO mice was undistinguishable (Kasper et al., 2005; Lange et al., 2006). As an alternative hypothesis, Wartosch et al. (Wartosch & Stauber, 2018) speculated that  $CIC-7$  exploits the large pH gradient to accumulate  $Cl^-$  necessary for activation of lysosomal hydrolases. Indeed,  $CIC-7$  KO mice displayed reduced luminal  $Cl^-$  concentration (Weinert et al., 2010). More recently, Wu et al. (2023) reported a prominent role of  $CIC-7$  for luminal  $Cl^-$  accumulation in phagosomes of macrophages. Their findings underscore the importance of high luminal  $Cl^-$  concentration for a wide range of phagosomal hydrolases (Wu et al., 2023). Similarly, in *C. elegans* carrying a gene defective for *clh-6*, corresponding to mammalian *CICn7* (Schriever et al., 1999), lysosomes acidified similar to wild type but displayed lower lysosomal  $Cl^-$  concentration and reduced activity of cathepsin B and L, key lysosomal cysteine proteases (Zhang et al., 2023).

In this scenario of lysosomal  $Cl^-$  accumulation, our finding of strong  $CIC-7$  activation by low  $Cl^-$ , or vice versa, inhibition of  $CIC-7$  by high luminal  $Cl^-$ , probably bears significant physiological implications. We speculate that  $CIC-7$  activity is required for  $Cl^-$  accumulation as long as intralysosomal  $Cl^-$  concentration is still low. Once this achieves a sufficient level,  $CIC-7$  activity then declines, thereby preventing  $Cl^-$  overload and osmotic swelling. In fact, at a membrane potential close to 0 mV, for a 1000-fold  $H^+$  gradient (pH gradient of 3 pH units), and assuming an intracellular  $Cl^-$  concentration of 30 mM (Sulis Sato et al., 2017), 2  $Cl^-/1 H^+$  exchange could accumulate  $Cl^-$  in equilibrium up to almost 1 M. The presence of numerous, large acidic vacuoles in cells of patients carrying the  $CIC-7^{Y715C}$  GoF variant might be explained by osmotic perturbation of lysosomal fission or fusion events. Both the  $FIG4$  phosphatase as well as the  $VAC14$  scaffolding protein function in the production of  $PI(3,5)P_2$ , and recently Cao et al. (2023) reported that mutants in either give rise to lysosomal enlargement and neurodegeneration that are partially rescued upon disruption of  $CIC-7$  function. Their findings align with a model whereby  $PI(3,5)P_2$  tonically inhibits  $CIC-7$  (Leray et al., 2022). On the other hand, disruption of  $CIC-6$  function in HAP1 cells lacking  $FIG4$  did not produce vacuolar enlargement. This observation argues against the notion that a similar mechanism produces accumulation of large vacuoles in cells overexpressing the  $CIC-6^{Y553C}$  GoF variant (Polovitskaya et al., 2020). This does not necessarily exclude a role for osmotic effects in producing the  $CIC-6^{Y553C}$  phenotype, even as it excludes dependence on elements of the  $PI(3,5)P_2$  regulatory machinery. Moreover, it is consistent with our observations that  $CIC-6^{Y781C}$  dependence on voltage –



as well as extracellular pH and Cl<sup>-</sup> – fundamentally resembles that of WT CLC-6.

We were surprised to find that the CLC-7<sup>R760Q</sup> mutation associated with dominant osteopetrosis and exhibiting accelerated gating kinetics relative to WT CLC-7 (Leisle et al., 2011), appeared indifferent to extracellular Cl<sup>-</sup>. Although more studies are needed to investigate this as well as other ‘gate accelerating’ osteopetrosis mutations (Di Zanni et al., 2021; Leisle et al., 2011; Sarttlet et al., 2014) in greater detail, altered Cl<sup>-</sup> sensitivity presents a key to a heretofore unrecognized mechanism for how these CLC-7 mutations cause disease.

To our knowledge, CLC-7 is the first CLC transporter family member inhibited by extracellular Cl<sup>-</sup> (Jentsch & Pusch, 2018). For all other CLC transporters, high extracellular Cl<sup>-</sup> enhances activity. The situation for CLC channels is more complex, because their gating depends on two different processes. On one hand, a protopore gate is mediated essentially by the gating glutamate, except in kidney CLC-K channels that lack the gating glutamate. In addition, a ‘common gate’ acts simultaneously on both protopores (Jentsch & Pusch, 2018). Very little is understood about the latter process, but it probably corresponds to the slow gating processes of CLC-7 (Ludwig et al., 2013) and of CLC-6. In both the prototypical *Torpedo* CLC-0 channel as well as the muscle CLC-1 channel, extracellular Cl<sup>-</sup> clearly activates common gating (Chen & Miller, 1996), similar to what we now report for CLC-6. Activation of CLC-7 by low extracellular Cl<sup>-</sup> is reminiscent of early reports of the effects of low extracellular Cl<sup>-</sup> on CLC-2 gating (Pusch et al., 1999). It will be interesting to explore if similar structural elements in CLC channels and transporters underlie the differential sensitivity of common gating to extracellular Cl<sup>-</sup>.

The extracellular pH dependence of CLC channel gating and that of CLC transporters present a more difficult comparison because of the complex interplay of protonation between the gating glutamate, extracellular histidine residues, and even a pore lysine residue (Jentsch & Pusch, 2018). Nonetheless, among the mammalian CLC-transporters, CLC-6 is the only one to be activated by low extracellular pH. It will be interesting to decipher the molecular mechanism underlying this atypical, but evidently important, behaviour.

## References

- Cao, X., Lenk, G. M., Mikusevic, V., Mindell, J. A., & Meisler, M. H. (2023). The chloride antiporter *CLCN7* is a modifier of lysosome dysfunction in *fig 4* and *vac14* mutants. *PLOS Genetics*, **19**(6), e1010800.
- Chen, T. Y., & Miller, C. (1996). Nonequilibrium gating and voltage dependence of the CLC-0 Cl<sup>-</sup> channel. *Journal of General Physiology*, **108**(4), 237–250.
- Di Zanni, E., Palagano, E., Lagostena, L., Strina, D., Rehman, A., Abinun, M., De Somer, L., Martire, B., Brown, J., Kariminejad, A., Balasubramaniam, S., Baynam, G., Gurrieri, F., Pisanti, M. A., De Maggio, I., Abboud, M. R., Chiesa, R., Burren, C. P., Villa, A., ... Picollo, A. (2021). Pathobiologic mechanisms of neurodegeneration in osteopetrosis derived from structural and functional analysis of 14 CLC-7 mutants. *Journal of Bone and Mineral Research*, **36**(3), 531–545.
- Friedrich, T., Breiderhoff, T., & Jentsch, T. J. (1999). Mutational analysis demonstrates that CLC-4 and CLC-5 directly mediate plasma membrane currents. *Journal of Biological Chemistry*, **274**(2), 896–902.
- Graves, A. R., Curran, P. K., Smith, C. L., & Mindell, J. A. (2008). The Cl<sup>-</sup>/H<sup>+</sup> antiporter CLC-7 is the primary chloride permeation pathway in lysosomes. *Nature*, **453**(7196), 788–792.
- Günther, W., Luchow, A., Cluzeaud, F., Vandewalle, A., & Jentsch, T. J. (1998). CLC-5, the chloride channel mutated in Dent's disease, colocalizes with the proton pump in endocytotically active kidney cells. *Proceedings of the National Academy of Sciences USA*, **95**(14), 8075–8080.
- Guzman, R. E., Grieschat, M., Fahlke, C., & Alekov, A. K. (2013). CLC-3 is an intracellular chloride/proton exchanger with large voltage-dependent nonlinear capacitance. *ACS Chemical Neuroscience*, **4**(6), 994–1003.
- Jentsch, T. J. (2007). Chloride and the endosomal-lysosomal pathway: Emerging roles of CLC chloride transporters. *The Journal of Physiology*, **578**(Pt 3), 633–640.
- Jentsch, T. J., & Pusch, M. (2018). CLC chloride channels and transporters: Structure, function, physiology, and disease. *Physiological Reviews*, **98**(3), 1493–1590.
- Kasper, D., Planells-Cases, R., Fuhrmann, J. C., Scheel, O., Zeitz, O., Ruether, K., Schmitt, A., Poet, M., Steinfeld, R., Schweizer, M., Kornak, U., & Jentsch, T. J. (2005). Loss of the chloride channel CLC-7 leads to lysosomal storage disease and neurodegeneration. *EMBO Journal*, **24**(5), 1079–1091.
- Kornak, U., Kasper, D., Bosl, M. R., Kaiser, E., Schweizer, M., Schulz, A., Friedrich, W., Dellling, G., & Jentsch, T. J. (2001). Loss of the CLC-7 chloride channel leads to osteopetrosis in mice and man. *Cell*, **104**(2), 205–215.
- Lange, P. F., Wartosch, L., Jentsch, T. J., & Fuhrmann, J. C. (2006). CLC-7 requires *Ostm1* as a beta-subunit to support bone resorption and lysosomal function. *Nature*, **440**(7081), 220–223.
- Leisle, L., Ludwig, C. F., Wagner, F. A., Jentsch, T. J., & Stauber, T. (2011). CLC-7 is a slowly voltage-gated 2Cl<sup>-</sup>/1H<sup>+</sup>-exchanger and requires *Ostm1* for transport activity. *EMBO Journal*, **30**(11), 2140–2152.
- Leray, X., Hilton, J. K., Nwangwu, K., Becerril, A., Mikusevic, V., Fitzgerald, G., Amin, A., Weston, M. R., & Mindell, J. A. (2022). Tonic inhibition of the chloride/proton antiporter CLC-7 by PI(3,5)P<sub>2</sub> is crucial for lysosomal pH maintenance. *Elife*, **11**, e74136.
- Ludwig, C. F., Ullrich, F., Leisle, L., Stauber, T., & Jentsch, T. J. (2013). Common gating of both CLC transporter subunits underlies voltage-dependent activation of the 2Cl<sup>-</sup>/H<sup>+</sup> exchanger CLC-7/*Ostm1*. *Journal of Biological Chemistry*, **288**(40), 28611–28619.

- Mellman, I., Fuchs, R., & Helenius, A. (1986). Acidification of the endocytic and exocytic pathways. *Annual Review of Biochemistry*, **55**, 663–700.
- Nicoli, E. R., Weston, M. R., Hackbarth, M., Becerril, A., Larson, A., Zein, W. M., Baker, P. R., 2nd, Burke, J. D., Dorward, H., Davids, M., Huang, Y., Adams, D. R., Zervas, P. M., Chen, D., Markello, T. C., Toro, C., Wood, T., Elliott, G., Vu, M., ... Malicdan, M. C. V. (2019). Lysosomal storage and albinism due to effects of a *De Novo* *CLCN7* variant on lysosomal acidification. *American Journal of Human Genetics*, **104**(6), 1127–1138.
- Piccolo, A., Malvezzi, M., & Accardi, A. (2010). Proton block of the ClC-5 Cl<sup>-</sup>/H<sup>+</sup> exchanger. *Journal of General Physiology*, **135**(6), 653–659.
- Piccolo, A., & Pusch, M. (2005). Chloride/proton antiporter activity of mammalian CLC proteins ClC-4 and ClC-5. *Nature*, **436**(7049), 420–423.
- Poët, M., Kornak, U., Schweizer, M., Zdebik, A. A., Scheel, O., Hoelter, S., Wurst, W., Schmitt, A., Fuhrmann, J. C., Planells-Cases, R., Mole, S. E., Hubner, C. A., & Jentsch, T. J. (2006). Lysosomal storage disease upon disruption of the neuronal chloride transport protein ClC-6. *Proceedings of the National Academy of Sciences USA*, **103**(37), 13854–13859.
- Polovitskaya, M. M., Barbini, C., Martinelli, D., Harms, F. L., Cole, F. S., Calligari, P., Bocchinfuso, G., Stella, L., Ciolfi, A., Niceta, M., Rizza, T., Shinawi, M., Sisco, K., Johannsen, J., Denecke, J., Carrozzo, R., Wegner, D. J., Kutsche, K., Tartaglia, M., & Jentsch, T. J. (2020). A recurrent gain-of-function mutation in *CLCN6*, encoding the ClC-6 Cl<sup>-</sup>/H<sup>+</sup>-exchanger, causes early-onset neurodegeneration. *American Journal of Human Genetics*, **107**(6), 1062–1077.
- Pusch, M., Jordt, S. E., Stein, V., & Jentsch, T. J. (1999). Chloride dependence of hyperpolarization-activated chloride channel gates. *The Journal of Physiology*, **515**(Pt 2), 341–353.
- Pusch, M., & Zifarelli, G. (2021). Large transient capacitive currents in wild-type lysosomal Cl<sup>-</sup>/H<sup>+</sup> antiporter ClC-7 and residual transport activity in the proton glutamate mutant E312A. *Journal of General Physiology*, **153**(1), e202012583.
- Sartetlet, A., Stauber, T., Coppieters, W., Ludwig, C. F., Fasquelle, C., Druet, T., Zhang, Z., Ahariz, N., Cambisano, N., Jentsch, T. J., & Charlier, C. (2014). A missense mutation accelerating the gating of the lysosomal Cl<sup>-</sup>/H<sup>+</sup> exchanger ClC-7/Ostm1 causes osteopetrosis with gingival hamartomas in cattle. *Disease Models & Mechanisms*, **7**(1), 119–128.
- Scheel, O., Zdebik, A. A., Lourdel, S., & Jentsch, T. J. (2005). Voltage-dependent electrogenic chloride/proton exchange by endosomal CLC proteins. *Nature*, **436**(7049), 424–427.
- Schrecker, M., Korobenko, J., & Hite, R. K. (2020). Cryo-EM structure of the lysosomal chloride-proton exchanger ClC-7 in complex with OSTM1. *Elife*, **9**, e59555.
- Schriever, A. M., Friedrich, T., Pusch, M., & Jentsch, T. J. (1999). CLC chloride channels in *Caenorhabditis elegans*. *Journal of Biological Chemistry*, **274**(48), 34238–34244.
- Smith, A. J., & Lippiat, J. D. (2010). Voltage-dependent charge movement associated with activation of the ClC-5 2 Cl<sup>-</sup>/H<sup>+</sup> exchanger. *The Federation of American Societies for Experimental Biology Journal*, **24**(10), 3696–3705.
- Stauber, T., & Jentsch, T. J. (2010). Sorting motifs of the endosomal/lysosomal CLC chloride transporters. *Journal of Biological Chemistry*, **285**(45), 34537–34548.
- Sulis Sato, S., Artoni, P., Landi, S., Cozzolino, O., Parra, R., Pracucci, E., Trovato, F., Szczurkowska, J., Luin, S., Arosio, D., Beltram, F., Cancedda, L., Kaila, K., & Ratto, G. M. (2017). Simultaneous two-photon imaging of intracellular chloride concentration and pH in mouse pyramidal neurons *in vivo*. *Proceedings of the National Academy of Sciences USA*, **114**(41), E8770–E8779.
- Ullrich, F., Blin, S., Lazarow, K., Daubitz, T., von Kries, J. P., & Jentsch, T. J. (2019). Identification of TMEM206 proteins as pore of PAORAC/ASOR acid-sensitive chloride channels. *Elife*, **8**, e49187.
- Wartosch, L., & Stauber, T. (2018). A role for chloride transport in lysosomal protein degradation. *Autophagy*, **6**(1), 158–159.
- Weinert, S., Jabs, S., Supancharit, C., Schweizer, M., Gimber, N., Richter, M., Rademann, J., Stauber, T., Kornak, U., & Jentsch, T. J. (2010). Lysosomal pathology and osteopetrosis upon loss of H<sup>+</sup>-driven lysosomal Cl<sup>-</sup> accumulation. *Science*, **328**(5984), 1401–1403.
- Wu, J. Z., Zeziulia, M., Kwon, W., Jentsch, T. J., Grinstein, S., & Freeman, S. A. (2023). ClC-7 drives intraphagosomal chloride accumulation to support hydrolase activity and phagosome resolution. *Journal of Cell Biology*, **222**(6), e202208155.
- Xu, H., & Ren, D. (2015). Lysosomal physiology. *Annual Review of Physiology*, **77**, 57–80.
- Zanardi, I., Zifarelli, G., & Pusch, M. (2013). An optical assay of the transport activity of ClC-7. *Scientific Reports*, **3**, 1231.
- Zhang, Q., Li, Y., Jian, Y., Li, M., & Wang, X. (2023). Lysosomal chloride transporter CLH-6 protects lysosome membrane integrity via cathepsin activation. *Journal of Cell Biology*, **222**(6), e202210063.
- Zifarelli, G., De Stefano, S., Zanardi, I., & Pusch, M. (2012). On the mechanism of gating charge movement of ClC-5, a human Cl<sup>-</sup>/H<sup>+</sup> antiporter. *Biophysical Journal*, **102**(9), 2060–2069.
- Zifarelli, G., Pusch, M., & Fong, P. (2022). Altered voltage-dependence of slowly activating chloride-proton antiport by late endosomal ClC-6 explains distinct neurological disorders. *The Journal of Physiology*, **600**(9), 2147–2164.

## Additional information

### Data availability statement

Upon reasonable request, the authors will make source data and materials available.

## Competing interests

No competing interests declared.

## Author contributions

M.C.: conception or design of the work; acquisition, analysis or interpretation of data for the work; drafting the work or revising it critically for important intellectual content; final approval of the version to be published; agreement to be accountable for all aspects of the work. P.G.: conception or design of the work; acquisition, analysis or interpretation of data for the work; final approval of the version to be published; agreement to be accountable for all aspects of the work. I.Z.: acquisition, analysis or interpretation of data for the work; drafting the work or revising it critically for important intellectual content; final approval of the version to be published; agreement to be accountable for all aspects of the work. A.T.-M.: acquisition, analysis or interpretation of data for the work; drafting the work or revising it critically for important intellectual content; final approval of the version to be published; agreement to be accountable for all aspects of the work. A.L.: conception or design of the work; drafting the work or revising it critically for important intellectual content; final approval of the version to be published; agreement to be accountable for all aspects of the work. P.F.: conception or design of the work; acquisition, analysis or interpretation of data for the work; drafting the work or revising it critically for important intellectual content; final approval of the version to be published; agreement to be accountable for all aspects of the work. M.P.: conception or design of the work; acquisition, analysis or interpretation of data for the work; drafting the work or revising it critically for important intellectual content; final approval of the version to be published; agreement to be accountable for all aspects of the work. All persons designated as authors qualify for authorship, and all those who qualify for authorship are listed.

## Funding

Fondazione AIRC per la ricerca sul cancro: Michael Pusch, IG 21558; Fondazione Telethon (FT): Michael Pusch, GMR22T1029; Fondazione Telethon/Cariplo: Michael Pusch, GJC22008; Kansas KINBRE: Peking Fong, P20 GM103418; KSU | College of Veterinary Medicine, Kansas State University SMILE: Peking Fong, Fong SMILE FY20; National Institutes of Health/National Institute of Neurological Disorders and Stroke: Peking Fong, 1R21NS131873-01.

## Acknowledgements

The authors gratefully acknowledge the expert technical assistance of Francesca Quartino and Alessandro Barbin, and constructive discussions with Dr Paola Imbrici. This work was supported by the Fondazione AIRC per la Ricerca sul Cancro (grant no. IG 21558), Fondazione Telethon (grant no. GMR22T1029), and Fondazione Telethon/Cariplo (grant no. GJC22008) to M.P. Also supported by the Kansas INBRE, P20 GM103418, the Kansas State University College of Veterinary Medicine, Fong SMILE FY20, and the National Institute of Neurological Disorders and Stroke, National Institutes of Health, United States of America, 1R21NS131873-01 to P.F.

## Keywords

chloride, CLC, homeostasis, lysosome, pH, transporters

## Supporting information

Additional supporting information can be found online in the Supporting Information section at the end of the HTML view of the article. Supporting information files available:

## Peer Review History